The Biomechanics of Musculoskeletal Tissues during Activities of Daily Living: Dynamic Assessment Using Quantitative Transmission-Mode Ultrasound Techniques

Scott C. Wearing [1,*], Sue L. Hooper [2], Christian M. Langton [3], Michael Keiner [4], Thomas Horstmann [1], Nathalie Crevier-Denoix [5] and Philippe Pourcelot [5]

1   School of Medicine and Health, Technical University of Munich, 80992 Munich, Bavaria, Germany
2   School of Health, University of the Sunshine Coast, Sippy Downs, QLD 4556, Australia
3   Griffith Centre of Rehabilitation Engineering, Griffith University, Southport, QLD 4222, Australia
4   Department of Exercise and Training Science, German University of Health and Sport, 85737 Ismaning, Bavaria, Germany
5   INRAE, BPLC Unit, Ecole Nationale Vétérinaire d'Alfort, 94700 Maisons-Alfort, France
*   Correspondence: s.wearing@tum.de; Tel.: +49-(89)-289-24566

Abstract: The measurement of musculoskeletal tissue properties and loading patterns during physical activity is important for understanding the adaptation mechanisms of tissues such as bone, tendon, and muscle tissues, particularly with injury and repair. Although the properties and loading of these connective tissues have been quantified using direct measurement techniques, these methods are highly invasive and often prevent or interfere with normal activity patterns. Indirect biomechanical methods, such as estimates based on electromyography, ultrasound, and inverse dynamics, are used more widely but are known to yield different parameter values than direct measurements. Through a series of literature searches of electronic databases, including Pubmed, Embase, Web of Science, and IEEE Explore, this paper reviews current methods used for the *in vivo* measurement of human musculoskeletal tissue and describes the operating principals, application, and emerging research findings gained from the use of quantitative transmission-mode ultrasound measurement techniques to non-invasively characterize human bone, tendon, and muscle properties at rest and during activities of daily living. In contrast to standard ultrasound imaging approaches, these techniques assess the interaction between ultrasound compression waves and connective tissues to provide quantifiable parameters associated with the structure, instantaneous elastic modulus, and density of tissues. By taking advantage of the physical relationship between the axial velocity of ultrasound compression waves and the instantaneous modulus of the propagation material, these techniques can also be used to estimate the *in vivo* loading environment of relatively superficial soft connective tissues during sports and activities of daily living. This paper highlights key findings from clinical studies in which quantitative transmission-mode ultrasound has been used to measure the properties and loading of bone, tendon, and muscle tissue during common physical activities in healthy and pathological populations.

Keywords: quantitative ultrasound; speed of sound; broadband ultrasound attenuation; connective tissue properties

1. Introduction

Musculoskeletal disorders, including injuries of bone, tendon, and muscle tissue, affect more than 1.71 billion people worldwide [1]. The loss of bone mass associated with osteoporosis, for instance, is estimated to affect more than 500 million adults worldwide, with approximately nine million reportedly suffering an osteoporosis-related bone fracture each year, equating to an osteoporotic fracture every three seconds [2,3]. Similarly, the

gradual loss of skeletal muscle mass and strength, characterizing sarcopenia, is conservatively estimated to affect as much as 10% of healthy older adults worldwide [4], while tendon disorders purportedly represent the primary musculoskeletal complaint for which a patient seeks medical attention [5]. Moreover, musculoskeletal disorders are a leading cause of chronic pain and protracted disability [6]. In 2020, musculoskeletal disorders were estimated to be the second-highest global cause of non-fatal disability [7]. Not surprisingly, musculoskeletal conditions are also the highest contributor to the global need for rehabilitation, with more than two-thirds of all adults worldwide in need of rehabilitative care [1].

The measurement of the mechanical properties of connective tissues and their change with physical loading is critical for understanding the cellular behavior of tissues, their normal 'homeostatic' tissue functionality, as well as the development of musculoskeletal disorders and their rehabilitation after injury [8]. The conceptual biomechanical model of the "mechanostat", first proposed by Harold Frost in the 1980s, is arguably among the most significant contributions to connective tissue research to date [9–11]. The model states that connective tissues, including bone, tendon, and muscle tissues, respond to habitual loading and that any change in the loading environment leads to the structural adaptation of tissue architecture. The model suggests the presence of a physiological feedback system, which is able to adjust tissue mass and structure according to the loads experienced. Cells play a pivotal role in the model, acting both as sensors as well as drivers of extracellular matrix synthesis and degradation. The mechanostat is typically modeled as a feedback algorithm using a set-point criterion based on a particular mechanical quantity, such as strain or strain rate. Although the precise set-point criterion for many musculoskeletal tissues, including bone, tendon, and muscle tissues, is the source of ongoing debate [12–16], these mechanical thresholds (set points), determine whether material is added to or lost from the tissue. Different muscles, tendons, and bones are thought to respond differently to increases or decreases in loading depending on the sensitivity of their specific mechanostat [17,18]. It is unclear why and how the different connective tissue structures respond to complex loading stimuli, which comprise numerous different parameters including strain magnitude, frequency, and rest intervals (among others). When mechanical stimuli fall below a certain mechanical set point, cell apoptosis occurs followed by tissue resorption. Conversely, when mechanical loading remains within certain set points, cells remain viable and no tissue is lost (i.e., homeostasis). With a greater than customary mechanical stimulus, cells release anabolic factors, resulting in tissue formation. With excessive mechanical stimuli, the accumulation of micro-damage is thought to exceed tissue formation, resulting in injury [14,19]. Hence, understanding tissue properties and the physiological loading governing the mechano-sensitization and desensitization of individual musculoskeletal tissue structures is essential for our ability to promote positive musculoskeletal adaptation, prevent injury, hasten its recovery after injury, and enhance performance.

The primary aims of this narrative review, therefore, were threefold. The first aim was to review conventional methods currently used to quantify the mechanical properties of human musculoskeletal tissues, such as bone, tendon, and muscle tissues, *in vivo*, as well as to highlight the strengths and limitations of each approach. The second aim was to broadly outline current transmission-mode ultrasound techniques that have been specifically developed to non-invasively quantify the mechanical properties of human musculoskeletal tissues, including a brief overview of their operating principles and key measurement parameters that are commonly used. The third aim was to review important findings from *in vivo* applications of each technique in quantifying the mechanical properties and biomechanical loading of bone, tendon, and muscle tissues, both at rest and during activities of daily living in clinical and non-clinical populations. We also highlight new and emerging applications before concluding with a brief precis of future directions for the development and potential applications of transmission-mode techniques to evaluate the human musculoskeletal system.

To meet the aims of this review, we conducted a series of broad literature searches of a variety of electronic databases, including Pubmed, Embase, Scopus, Web of Science, and IEEE Explore, between 30 June 2023 and 1 May 2024. Keyword searches were carried out for each section of this review and included, but were not limited to, the following terms, used in varying combinations with and without the use of wild cards, truncation, and Boolean operators: skeletal, musculoskeletal, connective tissue, bone, osseous, trabecular, cortical, tendon, muscle, quantitative ultrasound, transverse transmission, through transmission, axial transmission, pulse echo, ultrasound, speed of sound, attenuation, osteopenia, osteoporosis, muscle wasting, sarcopenia, cachexia, tendinopathy, tendon rupture, tissue properties, biomechanics, viscoelasticity, modulus, bone mineral density, apparent density, apparent density, Poisson's, and mechanobiology. No restrictions were placed on the publication date or type; hence textbooks, narrative and systematic review articles, meta-analyses, and original articles including, prospective and retrospective cohort studies, clinical trials, and observational studies, were included. A full-text review of sources was undertaken with respect to the hierarchy of the evidence and was limited to texts published in English or German languages. Additional sources were identified by scrutinizing the reference lists of published studies. In total, more than 800 peer-reviewed publications were retrieved and appraised, with 372 references directly included in the final review.

2. Conventional Methods for Characterizing Musculoskeletal Tissue Properties *In Vivo*

2.1. Bone

Dual-energy X-ray absorptiometry (DXA) is considered the current "gold-standard" method for assessing bone status *in vivo*. The technique quantifies the transmission and attenuation of two low-dose X-ray beams of separate energy, which are variably absorbed by hard and soft connective tissues, to provide a measure of areal bone mineral density (aBMD: g/cm^2); which is used as a surrogate measure of bone strength [20–22]. Although DXA is the most widely used technique for evaluating osteoporosis and fracture risk in adults, its use in quantifying bone properties has several limitations [23]. In particular, as the technique is reliant on a two-dimensional (2-D) projection of skeletal tissues, it is unable to provide reliable quantitative information regarding true (i.e., 3-D) volumetric bone mineral density (vBMD: g/cm^3) [24,25]. Moreover, normative data for aBMD have typically been reported only for common trabecular fracture sites, i.e., lumbar spine and hip [26], whereas 80% of osteoporosis-related fractures are estimated to involve the cortical bone [27]. Indeed, more than half of low-trauma fractures are reportedly undetected by DXA when the osteoporotic threshold defined by the World Health Organization (T-score = −2.5) is used [28], raising concerns regarding the sensitivity of DXA in detecting osteoporosis-related pathology [29,30]. In addition, the use of DXA in specific populations, such as children and adolescents, presents short-comings as DXA-based estimates of bone mineral density are highly dependent on bone morphology, body size, pubertal staging, and skeletal maturity [31]. Although high-resolution peripheral quantitative computed tomography (HR-pQCT) overcomes the 2-D limitations associated with DXA to provide 3-D information about cortical bone at peripheral skeletal sites [32,33], it currently provides insufficient spatial resolution to accurately evaluate intra-cortical porosity-related bone loss and involves the use of ionizing radiation, which limits its widespread use [34,35].

Likewise, the characterization of the *in vivo* loading environment of bones also presents significant technical challenges to researchers and clinicians. Although direct measurement methods, such as strain-gauge extensometry, have long been applied [36–38] and are widely considered to be the 'gold standard' for the assessment of bone and joint loading during physical activity [39], biomechanical models have been most commonly used. Typically informed by measurements of ground reaction force, muscle activity, motion analysis, and increasingly by inertial measurement units [40], various models have been constructed to estimate potential forces applied to appendicular and axial bones during walking, running, and jumping, among other activities [41–44]. However, the process involves multiple stages, each with assumptions and errors that can cause a much larger

compounded error [45]. As cautioned by Curry et al. [46], validation still represents a key limitation of many of the models that have been constructed. The advent of publicly available data sets, including direct measurements of joint contact force during walking (for example, [47,48]), has resulted in substantial improvement in the sophistication of modeling techniques [49], with the construction of patient-specific models, in particular, demonstrating encouraging accuracy for the estimation of the hip or tibiofemoral joint contact forces [50–52]. However, the extensive personalization of model parameters remains a time-consuming procedure and typically requires detailed medical imaging data that are not routinely available [53]. Thus, the capacity of validated musculoskeletal models to predict absolute contact forces during activities of daily living, other than walking-related tasks, has not been well studied [54,55].

2.2. Tendon

Several approaches for the non-invasive quantification of the mechanical properties of soft connective tissues, such as tendons, have been reported within the literature, including vibrational techniques [56–58], shear-wave elastography [59], and standard ultrasound imaging coupled with inverse dynamic models [60,61]. To date, most studies evaluating tendon properties have used standard B-mode ultrasonography coupled with inverse dynamics to indirectly estimate tendon displacement and loading commonly experienced during isometric muscle contractions (for example, [62,63]). The structural and material properties of the tendon, such as its stiffness, elastic modulus, and hysteresis, are then subsequently derived from either force–displacement or stress–strain curves. Although insightful, the indirect estimation of internal tendon properties using ultrasonography and inverse dynamics requires a number of key assumptions and has some significant limitations [64]. For instance, tendon loads derived from inverse approaches have been shown to be overestimated by as much as 50% compared to direct measurements [65,66], while estimates of viscous properties (hysteresis) have been shown to be physiologically implausible [67]. Indeed, direct measurements of the *in vivo* loading environment of human tendons have been made with relatively high accuracy via the use of implantable transducers, such as extensometer gauges, Hall-effect transducers, and fiber optic systems. The operating principles and limitations of each approach have been detailed elsewhere [68]. Although direct measurements of tendon force have been made during a number of activities of daily living, including walking, running, squatting, hopping, jumping, and cycling [69–77], these techniques are highly invasive, may interfere with normal movement patterns, often raise ethical concerns, and are commonly limited to small sample sizes. Moreover, to the best of our knowledge, they have not specifically evaluated mechanical loading in chronic tendon disease.

Shear-wave elastography, which has recently appeared in clinical settings, is among the better-established alternative modalities for quantifying the mechanical properties of muscles and tendons [78]. In contrast to standard ultrasound imaging and transmission-mode methods that use ultrasound compression waves, the technique estimates the material stiffness of tissues by measuring the velocity of shear waves rather than compression waves, which are typically generated either by the operator via the application of external forces or by an acoustic radiation force [79–81]. While elastography has been used for some time, with varying levels of success as a diagnostic aid in the assessment of chronic liver disease [81] and breast cancers [82], applications to musculoskeletal soft tissues are becoming increasingly popular [83–85]. By quantifying the velocity of the ultrasound shear wave, the technique has the potential to quantify the elastic modulus of tissues, which, subsequent to the non-linear properties of tendons at physiological loads [86,87], may also provide some insight into the internal loading environment of the tissue [59,88]. However, mathematical modeling studies have shown that longitudinal shear-wave velocity is unaffected by the tensile viscoelasticity of soft tissues [89,90], and thus, caution is required in its clinical use. Indeed, in a recent *ex vivo* study implementing both shear-wave and transmission-mode ultrasound methods, Glozman et al. [91] showed that estimates of

longitudinal shear-wave velocity, although strongly affected by the initial mechanical state of the tissue, were confounded by tissue non-linearity. This finding has been corroborated by animal studies, which observed no correlation between shear-wave velocity and the tensile elastic modulus of healthy rabbit Achilles tendons [92]. Similarly, in a recent *in vivo* study comparing shear-wave elastography with standard B-mode ultrasound coupled with inverse dynamics, Misfud et al. [93] noted that estimates of the tendon modulus were only moderately correlated (r = 0.64) and only at low levels of tendon loading (10% maximum voluntary contraction). Although there is some evidence that longitudinal shear-wave velocity in tendons may be sensitive to its strain-energy dissipation properties [94], shear-wave measurements have also been shown to be highly sensitive to confounders, and thus, reliability and reproducibility are thought to be greatly limited [95–97].

2.3. Skeletal Muscle

The characterization of the mechanical properties of skeletal muscle at the organ level is complicated by the contractile nature of the tissue. Some approaches have been proposed to measure the passive mechanical properties of skeletal muscle; however, there is little consensus within the literature concerning the most appropriate measurement method. Indeed, in the context of sarcopenia, a syndrome characterized by an accelerated loss of skeletal muscle mass and strength [98,99], many modalities have been used to characterize the "quantity," and to a lesser extent, the "quality," of skeletal muscle, including anthropometry [100], bioelectrical impedance analysis [101], DXA [102], ultrasound imaging [103], magnetic resonance imaging [104], and radiographic computed tomography [105,106]. The advantages and limitations of each modality, as they relate to the measurement of muscle mass, have been summarized elsewhere [107–109]. Arguably, the current reference standards for quantifying the passive mechanical properties of skeletal muscle tissue include radiographic computed tomography (CT) and magnetic resonance (MR) imaging, which are capable of providing high-resolution cross-sectional images that allow the differentiation between skeletal muscle and other lean mass components [110–112]. Measurements of cross-sectional skeletal muscle area or volume, which are often allometrically scaled to measurements of body height, can be subsequently made to yield relative estimates of muscle mass, such as the skeletal muscle index (cm^2/m^2) [113]. Surrogate estimates of muscle composition and quality may also be obtained on the basis of signal intensity or the diffusion anisotropy of water in the case of MR imaging or with the transformation of attenuation coefficients to radio densities in the case of CT, which reportedly relate to muscle fat content [104,114]. MR imaging has also been applied in elastographic approaches as a measure of passive skeletal muscle properties [108]. As with ultrasound-based elastography, MR elastography relies on the transmission of an external vibration through skeletal muscle but uses MR imaging to measure the subsequent propagation of displacement waves through the tissue. Maps of shear modulus are then calculated based on the linear viscoelastic wave equation. A review of the technical details of the approach is provided elsewhere [115]. To date, the majority of MR elastography studies have assumed muscle to be isotropic [116–118]. Anisotropic approaches require additional information regarding muscle fascicle architecture, which can, for instance, be obtained from diffusion imaging [119,120]. Such methods have been used to study the elastic and viscous properties of both healthy and disease-affected muscles in their passive state [120–122]. While MR elastography is generally considered more reliable than ultrasound elastography [123–125], there is growing evidence that it may also be sensitive to contraction-induced stiffness changes, primarily at low levels of muscle contraction [116,122,126,127], which may contribute to lower apparent reliability [108]. Moreover, the typical scan duration and physical restrictions associated with MR elastography make it impractical to measure changes in the mechanical properties of skeletal muscle during "real-world" dynamic activities of daily living, such as walking, running, and stair climbing [127].

The force-generating capacity of skeletal muscle is most commonly estimated *in vivo* using simple dynamometry. Given the well-established relationship between muscle size

and maximum voluntary force output [128,129], dynamometric measurements of skeletal muscle strength or torque are often normalized to image-based measurements of muscle volume or cross-sectional area to yield relative measurements of muscle strength. It is well known, however, that increases in strength do not necessarily correspond to increases in skeletal muscle mass [130] and that force generation in skeletal muscle is the result of a number of additional factors, including tissue composition (e.g., contractile versus non-contractile), architecture (intramuscular fiber orientation, length, and pennation), and neural activation (such as motor unit recruitment patterns, central drive, etc.), that contribute to the overall force production capabilities [131–133]. Hence, while electromyography has been used to estimate skeletal muscle force [134], electromyography-based estimates of muscle force can be substantially inaccurate [135]. Arguably, the estimation of the "specific tension" of a muscle (the maximal force per unit of physiological cross-sectional area) [136,137] may be a more appropriate indicator of the contractile quality of skeletal muscle. However, such estimates typically require the combined use of multiple modalities (dynamometry, ultrasound, MR, electrostimulation, and electromyography) to address issues related to the variation in motor unit recruitment, central drive, and participant motivation, to quantify muscle architecture, joint centers, and moment arms, and to address assumptions regarding agonist and antagonist muscle contributions to the net joint moment, each of which has errors that can result in considerable compounded errors [138] and that may partly underpin the wide variation in specific tension, for example, from 150 kPa [136] to 540 kPa [139], reported for human skeletal muscle measured *in vivo*.

3. Techniques for Quantitative Transmission-Mode Ultrasound

Although ultrasound compression waves have long been used for the non-destructive characterization of defects in engineering materials, first appearing in the 1930s [140], it was not applied in humans for the evaluation of musculoskeletal tissue properties until 1958, when it was first used, with limited success, to evaluate cortical bone status during fracture healing [141]. However, it was some 25 years later that the clinical utility of quantitative ultrasound was demonstrated with the publication of the seminal work of Langton et al. [142], in which transmission-mode ultrasound was used to assess cancellous bone.

In contrast to the qualitative information commonly afforded by the visual observation of ultrasound waveforms in A-mode, tomographic images in B-mode, and dynamic images in M-mode, quantitative transmission-mode ultrasound evaluates the fundamental properties of musculoskeletal tissue based on the interactions of propagating ultrasound compression waves with the tissue microstructure [143–145]. Indeed, the propagation characteristics of ultrasound compression waves through musculoskeletal tissues have been shown to be related to the mechanical properties (elastic coefficients) of the tissue, as well as to other characteristics, including mass density and macro- or microarchitecture, which, in turn, are associated with biomechanical properties [146–150]. Hence, quantitative ultrasound techniques, such as transmission-mode ultrasound, have been used to assess the material and structural properties of connective tissues and their change with loading, providing new insights into the health of musculoskeletal tissues and the biomechanical control of activities of daily living.

Transmission-mode techniques using ultrasound compression waves may be generally classified into one of three categories (Figure 1): 1. through- or transverse-transmission, 2. pulse-echo, and 3. axial-transmission. While the current paper provides a brief overview of the operating principles behind each technique, a comprehensive discussion concerning the equipment, operating principles, analytic approaches, and limitations associated with each one and their many variants have been detailed elsewhere [151–153].
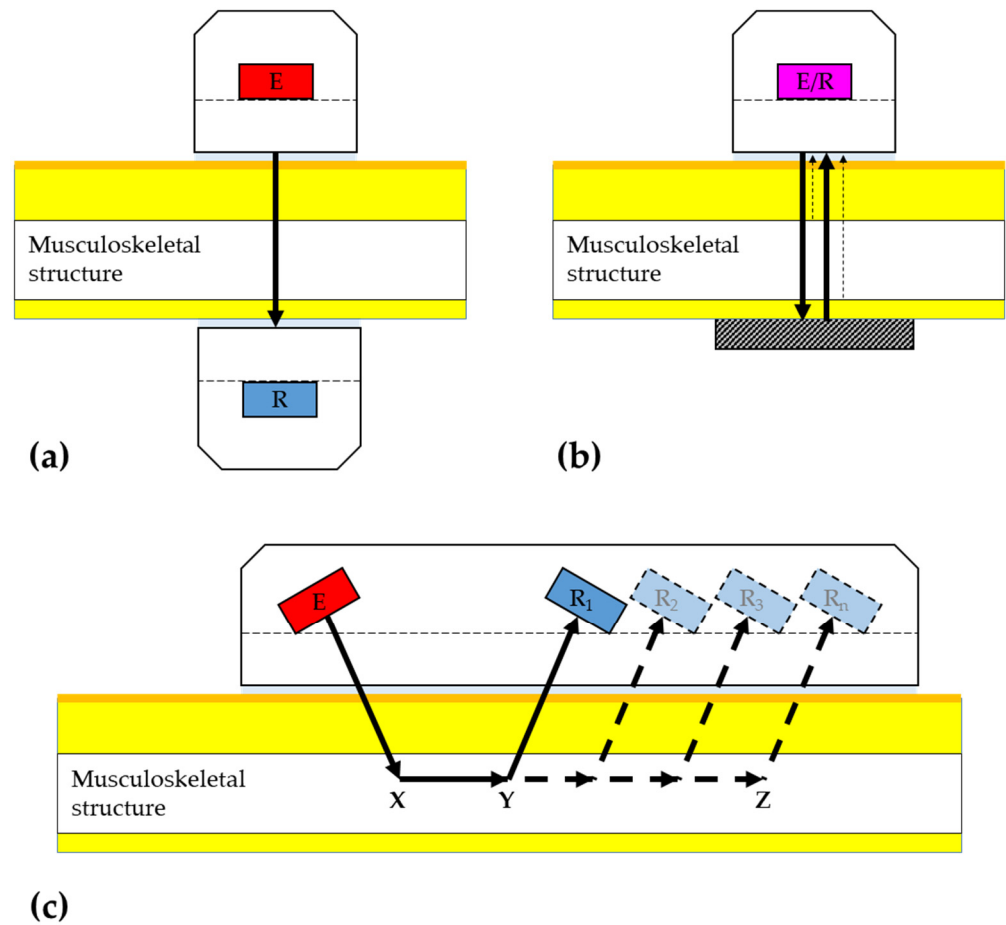
Figure 1. Illustration of the basic setup and operating principles of classical transmission-mode ultrasound techniques. (**a**) In the through-transmission technique, two ultrasound transducers, i.e., an emitter (E: red) and a receiver (R: blue), are placed on opposing sides of the musculoskeletal structure and provide estimates of tissue properties in the transverse plane. (**b**) Pulse-echo transmission approaches use a single ultrasound transceiver (E/R), operating in transmit and receive modes. Tissue characteristics are estimated by evaluating the backscattered signal and typically require assumed knowledge or combined measurements of one or several material properties. In soft tissues, the approach is often used in combination with a reflector (gray) positioned at a known distance from the transceiver. (**c**) Axial-transmission techniques typically employ two or more linearly orientated and regularly spaced ultrasound transducers consisting of an emitter (E: red) and one or more receivers (R: blue) aligned along the same side of the musculoskeletal structure. A broadband ultrasound pulse enters the musculoskeletal structure at a critical angle, and the compression wave propagates along the long axis of the structure.

3.1. Through-Transmission Techniques

The through-transmission technique uses a separate emitter and a collinearly aligned receiver positioned on opposite sides of the musculoskeletal structure to be measured (Figure 1a). The distance between the emitter and receiver is either known or measured. Assuming that the system response and wave propagation are linear, the transmission characteristics, such as attenuation and velocity, of a broadband ultrasonic excitation transmitted through the sample can be readily obtained using the classical substitution technique, in which the signal transmitted through the musculoskeletal site is compared to that transmitted through a reference medium, such as water, at a known temperature [142,144,152].

3.2. Pulse-Echo Transmission Techniques

In contrast to through-transmission, pulse-echo transmission uses a single ultrasound transceiver, operating in both transmit and receive modes. Upon entering the skin and subcutaneous tissues, the broadband ultrasonic pulse is scattered and reflected from point-normal orientated interfaces where there is an acoustic mismatch between media, passes through mutual interference, and is received by the transceiver as radiofrequency echo signals (Figure 1b). Key characteristics of the target tissue, such as its thickness and attenuation, are subsequently estimated by evaluating the backscattered signal, which returns along the same path as the transmission [154–156]. In general, pulse-echo measurements of musculoskeletal tissues *in vivo* rely on assumed or a priori knowledge or combined measurements of one or several material properties, such as ultrasound velocity [153]. In some instances, an external reflector of a known distance from the transceiver is employed, thereby minimizing the need for prior knowledge [157,158].

3.3. Axial-Transmission Techniques

The axial-transmission technique, in contrast, uses two or more transducers, one acting as an emitter and the others as receivers [159]. The regularly spaced transducers are linearly orientated and axially aligned along the same side of the musculoskeletal structure to be measured (Figure 1c) [147]. Axial wave propagation differs considerably from conventional through-transmission and pulse-echo measurements. A broadband ultrasonic excitation is transmitted through the subcutaneous tissue and enters the musculoskeletal structure at a critical angle [160]. The refracted wavefront propagates along the longitudinal axis of the structure and, in doing so, results in a lateral wave that radiates into the subcutaneous tissue at a critical angle [161]. The transit time of the first arriving lateral wavefront along a defined distance is measured and used to calculate velocity. When applied to structures thicker than the involved wavelength, the apparent velocity of ultrasound in axial transmission corresponds to the speed of compressional bulk wave within the musculoskeletal structure [161,162]. The use of two or more receivers makes it possible to overcome the influence of the overlying skin and materials on the front of the probe when calculating wave speed [147,163]. As illustrated in Figure 1c and shown through Equations (1)–(6), the Time of Flight (ToF, in s), defined as the time the lateral wave of ultrasound pulse takes to travel along its transmission pathway, is measured at each receiver. The axial velocity is subsequently calculated by dividing the known distance between receivers by the ToF.

$$ToF_{R_1-R_n}(\text{s}) = ER_n\,(\text{s}) - ER_1\,(\text{s}) \tag{1}$$

$$\text{where, } ER_1\,(\text{s}) = EX(\text{s}) + XY(\text{s}) + YR_1(\text{s}) \tag{2}$$

$$ER_n\,(\text{s}) = EX(\text{s}) + XZ(\text{s}) + ZR_n(\text{s}) \tag{3}$$

$$\text{as, } YR_1(\text{s}) = ZR_n(\text{s}) \tag{4}$$

$$ToF_{R_1-R_n}(\text{s}) = XZ(\text{s}) - XY(\text{s}) \tag{5}$$

$$\text{which simplifies to } To\,F_{R_1-R_n}(\text{s}) = YZ(\text{s}) \tag{6}$$

3.4. Key Transmission-Mode Measurement Parameters

The two most common parameters measured using transmission-mode ultrasound techniques are the propagation velocity (V, in m/s) and attenuation, reported either at a single frequency (α, in dB/m) or as frequency-dependent attenuation (FDA, in dB/MHz/m). From these measurements, a number of composite measurements have also been derived, particularly for bone, which have been reviewed elsewhere [164].

The longitudinal velocity of an ultrasound wave (*V*) in musculoskeletal tissues is dependent on the instantaneous elastic modulus (*E*) and mass density (*ρ*) of the tissue through which it propagates and is governed by the following relationship [143,149,165,166]:

$$V = \sqrt{\frac{E}{\rho}}\ \mathrm{k} \tag{7}$$

where k is a constant relating to Poisson's effects and the negative ratio of axial to transversal strain with loading, which for connective tissues, such as tendons, is independent of the applied load [167]. Moreover, in soft connective tissues, which typically operate within the so-called 'toe region' under physiological loads, the axial velocity of ultrasound can be used as a surrogate measure of elastic modulus as it has been shown to vary monotonically with the applied load [148,149,168–170]. Hence, although the change in ultrasound velocity with loading represents a limitation of most sonographic approaches used to characterize soft-tissue properties [171], transmission techniques take advantage of this relationship, along with the non-linear properties of soft connective tissues at physiological loads [86,87], to also quantify the loading of soft tissues *in vivo* during dynamic activities of everyday living [172–174].

The propagation of ultrasound waves through tissue also results in a loss of signal intensity or attenuation via a number of processes, including both viscous and relaxation absorption [175], scattering, reflection [176], diffraction [177], mode conversion, and phase cancellation [152,178]. The loss of intensity or apparent attenuation (*α*) can be obtained from the referent (*A_{ref}*) and measured sample (*A_{sample}*) signals in either the time or frequency domain using the following equation [179]:

$$\alpha = 20 \ln \frac{\left| A_{ref} \right|}{\left| A_{sample} \right|} \tag{8}$$

At the frequency range commonly used *in vivo*, ultrasound attenuation in musculoskeletal tissues typically varies quasi-linearly with frequency [180,181], with attenuation over the 0.2–0.6 MHz frequency range commonly referred to as broadband ultrasound attenuation (BUA) [144]. Table 1 shows the approximate ultrasound velocity, attenuation, tissue density, and elastic modulus values of muscle, tendon, and bone samples.

Table 1. Approximate values * reported for ultrasound velocity, attenuation, density, and elastic modulus of muscle, tendon, and bone.

Tissue	Velocity (m/s)	Attenuation (dB/MHz/cm)	Density (g/cm^3)	Elastic Modulus (GPa)
Bone	2700–4100 [182,183]	2–15 [†] [182–184]	1.38–1.81 [182]	6.9–20.7 [46,185,186]
Cortical	2660–4200 [185,187,188]	5–12 [‡] [189]	1.66–2.10 [185,187,188]	10.9–19.7 [188]
Cancellous	1517–2892 [185,187,189,190]	4–31 [190]	1.08–1.76 [187,191]	3.0–15.0 [192]
Tendon	1637–1938 [143,168,187,193]	2–5 [184,193]	1.06–1.17 [149,168,187]	0.9–2.0 [60,194]
Muscle	1545–1631 [183,187,195–198]	0–3 [183,195–199]	1.04–1.18 [183,187,195,196]	0.1–0.4 [8,200]

* Approximate values vary with intrinsic, extrinsic and measurement-related factors including age, temperature and orientation. [†] dB/cm measured at 1 MHz. [‡] Radial measurement.

4. *In Vivo* Application of Transmission-Mode Ultrasound

4.1. *Measurement of Bone Properties*

All three ultrasound transmission techniques (i.e., through-transmission, pulse-echo, and axial-transmission techniques) have been used in the evaluation of passive properties of human bone, primarily within the context of osteoporosis and fracture risk. While each technique has been applied to a variety of skeletal sites, the increasing number of commercially available devices, which differ in terms of their measurement parameters coupled with the absence of technology-specific guidelines, has limited the widespread acceptance of transmission-mode ultrasound for the determination of passive bone properties for osteoporotic fracture risk within clinical settings [201]. The most common applications of each technique, however, are briefly reviewed below.

The earliest and arguably best-validated approach in bone involves through-transmission measurements [201]. The majority of research employing the through-transmission technique has evaluated the calcaneus due to its high trabecular content, metabolic activity, and similar demineralization pattern to that of vertebrae [202,203]. However, the method has also been applied to evaluate the bone status of the proximal femur [204], patella, distal tibia, ulnar, radius, and phalanges [205–208], with the latter generally considered a measure of cortical properties (i.e., "cortical transverse transmission") [209,210]. As shown in Figure 2a, measurements of ultrasound velocity are site-specific. In one of the earliest studies, Gerlanc et al. [208] reported ultrasound velocity through the distal tibia and ulna utilizing a through-transmission technique; the measurements were performed at regions of relatively constant and minimal soft-tissue thickness between the tibial tubercle and medial malleolus and between the olecranon and ulnar styloid, respectively. The ultrasound velocity values for both tibia and ulna in males demonstrated a rise from the third decade to the fourth decade, with a gradual decline thereafter. In contrast, females exhibited an increased ultrasound velocity at the tibia and ulna from the third decade to the fifth decade, followed by a greater decline in ultrasound velocity with age. The ultrasound velocity in people with an overt fracture at the tibia initially decreased but then increased non-linearly with healing. Delayed-union was characterized by a longer period of reduced ultrasound velocity before gradually increasing.
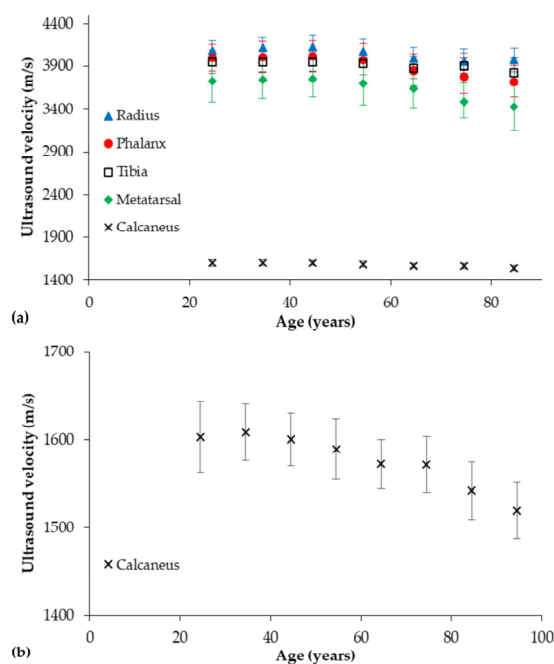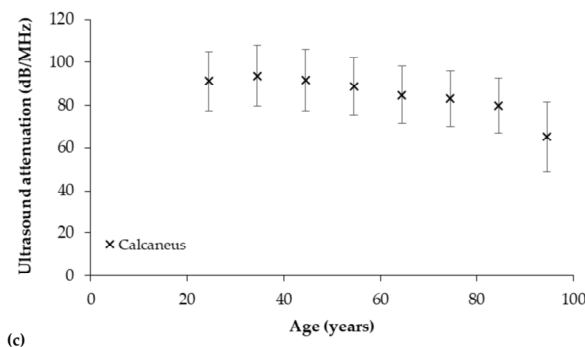

Figure 2. *Cont.*

(c)

Figure 2. (**a**) Mean ultrasound velocity of the radius, phalanges, tibia, and calcaneus reported in healthy adults (n = 2969) [211–215]. Note that measurements of ultrasound velocity are site-specific. (**b**) Mean ultrasound velocity and (**c**) attenuation reported at the calcaneus as a function of chronological age in cross-sectional studies of healthy adults (n = 1836) [211–213]. The error bars depict the standard deviation.

Ex vivo studies employing the through-transmission technique to evaluate trabecular bone have long since demonstrated that ultrasound velocity is closely related to its elastic modulus and, to a lesser extent, mass density [188,216]. Overall, similar age-related changes in ultrasound velocity profiles to those noted in the ulna and tibia [208] have been reported with trough-transmission measurements of the calcaneus in male and female populations (Figure 2b). In contrast to measurements of ultrasound velocity, measurements of ultrasound attenuation are thought to primarily reflect indices of bone mineral density and trabecular microarchitecture [217–223]. Langton et al. [142], in seminal work that greatly influenced later developments, applied the through-transmission technique to demonstrate, for the first time, that the slope of frequency-dependent attenuation of ultrasound at the calcaneus could be used to discriminate osteoporotic from non-osteoporotic individuals. Subsequent research demonstrated that, similar to measurements of velocity, ultrasound attenuation was sensitive to the effects of senescence, showing a reduction in attenuation values after the third decade (Figure 2c). Further research involving cross-sectional and longitudinal cohorts has provided considerable evidence that through-transmission measurements of ultrasound velocity and attenuation at the calcaneus are predictive of vertebral and femoral neck fractures in osteoporotic and several non-osteoporotic groups [224–229], with predictive rates comparable to or higher than that of radiographic-based measurements of bone mineral density [224,228,230–232]. They have also been shown to be predictive of low-trauma fractures in people with type 2 diabetes and chronic kidney disease [231,233], in which traditional X-ray-based clinical tools are generally considered insensitive [234].

A recent study of the UK Biobank, which includes over half a million adults recruited via the National Health Service, has also shown that calcaneal ultrasound velocity measured using the through-transmission technique is also independently associated with measurements of blood vessel compliance [235]. More recently, it was shown that broadband ultrasound attenuation of the calcaneus, but not apparent ultrasound velocity, was an independent predictor of both cardiovascular and all-cause mortality, even after adjustment for established cardiovascular risk factors and hip BMD [236], highlighting the potential utility of calcaneal ultrasound velocity to also evaluate the risk of cardiovascular disease.

Axial-transmission approaches have also been specifically advocated for use in osteoporosis [237] since approximately 80% of fragility fractures involve the appendicular skeletal sites comprised of large amounts of cortical rather than trabecular bone [27]. Cortical thinning and increased intra-cortical porosity are key factors underpinning non-vertebral fracture risk [238,239], and apparent ultrasound velocity in axial transmission is partly dependent on intra-cortical porosity, mineralization, and cortical bone thickness relative to its wavelength [161,240]. The technique has been most commonly applied to evaluate the cortical properties of long bones including the radius, tibia, metatarsus, and phalanges [240–242]. Although the level of evidence supporting the use of through-transmission ultrasound of

the calcaneus for evaluating fracture risk is considerably greater than for other transmission modes, there is compelling evidence that axial-transmission parameters are also capable of discriminating between individuals with an osteoporotic fracture (in the hip, vertebrae, or other site) from age-matched healthy individuals [160,243–247]. Current evidence from prospective studies, however, is generally mixed [248–251], with a recent prospective study of children suggesting that through-transmission-derived measurements of calcaneal ultrasound attenuation may be superior to axial-transmission measurements of tibial velocity for monitoring bone densitometric change during puberty [252]. Although tibial ultrasound velocity has been shown to reflect the strength and elastic modulus of cortical bone [253] and is correlated with tibial bone mineral density, and, to a lesser extent, mineral density at other skeletal sites [237], it has also been shown to be a poor discriminator of osteoporotic fracture [254].

Axial-transmission ultrasound has also been applied as a quantitative method to evaluate fracture healing in long bones. Indeed, the technique was first developed in 1958 to study cortical bone status during fracture healing, albeit with limited success [141]. As described by Bossy et al. [162], the application of the axial-transmission technique to cortical bone yields both a fast-moving axial compression wave and slower "guided" waves. The latter waves arise from the reflection, mode conversion, and interference of longitudinal and shear waves within the cortical structure [241]. Animal, simulation, and clinical studies have demonstrated that axial-transmission parameters, such as the time of flight and propagation velocity of the first arriving ultrasound signal (i.e., fast wave), when measured across a fracture site, can be used as an indicator of bone fracture and healing [162,208,255–257], with propagation velocity, rather than attenuation, being arguably more sensitive to changes in callus mineralization and porosity during the regeneration process [258,259]. Similarly, simulation and *ex vivo* studies have also suggested that guided waves, which are generally dispersive and influenced by both the periosteal and endosteal bone surfaces, may be even more useful for evaluating oblique and transverse fractures in cortical bone [241,260–263] and may even have the potential to detect osseous micro-cracks [264]. The technique also allows waveguide characteristics of the bone, such as cortical thickness and/or porosity, to be estimated from dispersion curves by fitting a theoretical waveguide model [265–268]. Although preliminary applications *in vivo* show promise [269,270], soft tissue properties, multimode overlap, and the conversion of guided waves still present a significant challenge for the routine *in vivo* use of ultrasonic guided waves for the quantification of cortical bone fracture [271,272]. Moreover, further prospective research studies are needed to demonstrate the clinical potential of axial-transmission techniques for quantifying fracture characteristics in cortical bone and the subsequent healing stages.

In one of the earliest clinical studies, Craven et al. [273] reported ultrasound velocity in the cortical bone of the radius utilizing a pulse-echo technique, dividing bone thickness derived from plain radiographs by measured ultrasound transit time. A small cohort of nine adult males (23–33 years) exhibited larger cortical thickness and ultrasound velocities than 11 female adults aged between 49 and 71 years. In a subsequent paper [274], the elastic modulus was estimated as the square of ultrasound velocity multiplied by bone density, derived using both plain radiograph and photon absorptiometry data. The same research group also presented a conference abstract reporting a pulse-echo method to estimate ultrasound attenuation in cortical bone, derived from measurements of inner and outer cortices at two sites of different cortical thicknesses [275]. Given that cortical porosity and thickness are important determinants of the mechanical properties of the bone [276,277], pulse-echo methods have more recently been employed to estimate transverse ultrasound velocity, cortical thickness, and osteoporotic fracture risk. Primarily targeting cortical bone sites, including the distal radius and tibia, the simplest approach estimates cortical thickness using a single-element pulse-echo configuration to record the time lag between reflections from the periosteal and endosteal interfaces of the distal radius. The apparent cortical thickness is subsequently derived based on the assumptions of a normal-incidence

homogenous material with perfectly flat interfaces and a priori knowledge of an invariant radial ultrasound velocity [155,278]. The technique also assumes that specular reflections from periosteal and endosteal cortical interfaces are stronger than backscattered ultrasound signals from cortical pores. Nonetheless, when combined with basic anthropometric data, multi-site pulse-echo thickness estimates were reported to have varied sensitivity (80–94%) and specificity (60–88%) in identifying hip osteoporosis compared to DXA but did not enhance the identification of radiographically confirmed fractures compared to estimates based on age and bone mineral density alone [279–283].

Ultrasound backscatter parameters, which can also be obtained from pulse-echo measurements, have also been applied to explore bone quality at both cortical- and trabecular-rich sites [284–286]. Backscatter occurs as the ultrasonic pulse interacts with the porous microstructure of bone, namely solid–fluid impedance mismatches, to provide frequency-dependent information on the composition (5 MHz), structure, and mechanical properties (1–3 MHz) of the bone [285,287–289]. Case-control studies have suggested that, compared to DXA, backscatter approaches applied *in vivo* to axial and appendicular reference sites can generally distinguish between elderly adults with and without osteoporosis, albeit with varied sensitivity (65–92%) and specificity (74–95%) [290–295]. Research has also demonstrated the utility of pulse-echo backscatter parameters in identifying fragility fractures [281,296,297], with several prospective studies reporting predictive metrics for fractures of the hip, spine, and "all" sites comparable to, or better than, DXA [298,299].

Although some pulse-echo backscatter approaches are reportedly limited by non-uniformities in the acoustic near-field [300], preliminary longitudinal studies suggest that backscatter parameters are also sufficiently sensitive to detect changes in cortical and trabecular bones following extended (90 days) bed rest [301], with a sensitivity comparable to that of axial-transmission techniques [302]. Although pulse-echo backscatter approaches also show promise for monitoring neonatal bone status [303,304], prospective research studies are needed to evaluate the sensitivity of pulse-echo techniques to quantify early skeletal changes with growth and metabolic disease and following therapeutic intervention.

4.2. Measurement of Bone Loading

The majority of research undertaken to date has applied transmission-mode ultrasound techniques to evaluate the passive material and structural properties of the bone. In one of the few studies evaluating the effect of mechanical loading on bone properties, Liu et al. [305] reported that through-transmission measurements of ultrasound attenuation at the calcaneus were significantly reduced with body-weight loading in a group of pre- and postmenopausal women (n = 16 and 45, respectively). While measurements of ultrasound velocity were also increased with loading, albeit to a lesser extent, the authors noted that the loading-induced reduction in ultrasound attenuation was greater in postmenopausal than premenopausal women. The authors suggested that greater ultrasound attenuation likely reflected changes in the trabecular microarchitecture with body-weight loading, highlighting the potential of the technique to evaluate the mechanical response of the bone to loading during activities of daily living. With the exception of heavily demineralized bone, however, mechanical testing of whole bone specimens *ex vivo* typically does not demonstrate an initial period of non-linear deformation with loading [306,307], the so-called "toe region", which is characteristic of soft tissues and facilitates the use of the technique for quantifying the dynamic loading of soft tissues. Moreover, preliminary work from our laboratory has also highlighted that body-weight loading results in a change in the orientation of the calcaneal bone and differential movement of the overlaying soft tissues, resulting in small changes in the location of measurements [308]. Indeed, it is well known that the orientation of the bone and thickness of the overlaying soft tissue can significantly affect clinical measurements of broadband ultrasound attenuation of the calcaneus when using the through-transmission approach, albeit such effects are more pronounced for measurements of calcaneal ultrasound velocity [309–313]. Moreover, in

contrast to ultrasound velocity, an established theoretical relationship linking ultrasound attenuation to the mechanical properties of the bone remains elusive [152,314].

4.3. Measurement of Tendon Properties

Although through-transmission techniques were applied as early as the 1990s to quantify the interaction and dispersive effects of the equine tendon on the propagation characteristics of ultrasound waves *ex vivo* [143,315], it was not until a decade later that axial-transmission techniques were first applied to evaluate human tendon biomechanics *in vivo* [148,172]. By measuring the transmission velocity of ultrasound compression waves along (as opposed to across) the tendon, axial-transmission ultrasound is particularly well suited to evaluating dynamic tendon biomechanics *in vivo* and has been successfully applied in a series of human cohort studies to evaluate tendon biomechanics during static and dynamic loading conditions [172–174,316–318], in tendon pathology [174,316,319], and common clinical approaches used to modify tendon loading [320–323], as outlined below.

4.3.1. Tendon Biomechanics during Common Activities of Daily Living

Axial-transmission techniques employing a nominal 1 MHz ultrasound emitter have typically been used to quantify the acute change in Achilles tendon (Figure 3a) and, to a lesser extent, patellar tendon properties during activities of daily living. During each heel–toe walking cycle, the axial ultrasound velocity trace in the Achilles tendon is characterized by two minima and two maxima (Figure 3b). The first minimum occurs shortly after the heel strike, at approximately 10% of the stance, following peak ankle plantarflexion, before peaking in the late stance at around 50% of the gait cycle shortly after peak vertical ground reaction force. The second and more profound minimum in ultrasound velocity occurs during the early swing phase at around 70% of the gait cycle before peaking again shortly prior to the next heel strike. The biphasic pattern was shown to be highly reproducible, with within-subject coefficients of variation typically <1.5% [317,320], and comparable to directly measured force profiles previously reported in the Achilles tendon with implanted force transducers [69,72,75]. While our unpublished data indicate that between-limb differences in axial velocity in the Achilles tendon during walking at preferred speeds are typically <1.5%, subsequent research has shown that increasing walking speed (0.85–1.35 m/s) resulted in a speed-dependent reduction in the axial velocity of ultrasound in the Achilles tendon during the stance phase of walking (Figure 3b), despite a concomitant increase in peak vertical ground reaction force and ankle plantarflexion [173]. The observation of a speed-dependent reduction in ultrasound velocity in the Achilles tendon is in close agreement with those in which force was directly measured within the tendon (Figure 3b inset) [72,75]. Although consistent with the limitations in the force–velocity behavior of the triceps surae muscle group [324], gait speeds associated with running were found to induce higher peak ultrasound velocities than for walking and, hence, higher internal loads within the Achilles tendon [317].

Subsequent research demonstrated that the foot-strike pattern adopted by runners had a profound effect on the axial ultrasound velocity recorded in the tendon during running (Figure 3c), with habitual forefoot-strike running patterns showing higher and earlier peak velocities than habitual rearfoot strikers [325]. The magnitude of the foot-strike effect (≈150 m/s) was marked compared to changes observed with walking speed but similar to that (≈140 m/s) observed with surgically induced injuries in the equine tendon [326]. Moreover, in comparison to habitual rearfoot strikers, runners that habitually adopted a forefoot-strike pattern also had markedly higher velocities in the tendon during walking (≈100 m/s) even though both groups adopted the same heel–toe walking pattern (Figure 3d). Hence, these findings highlighted that habitual footfall patterns during running may influence the functional properties of the Achilles tendon in recreational runners.
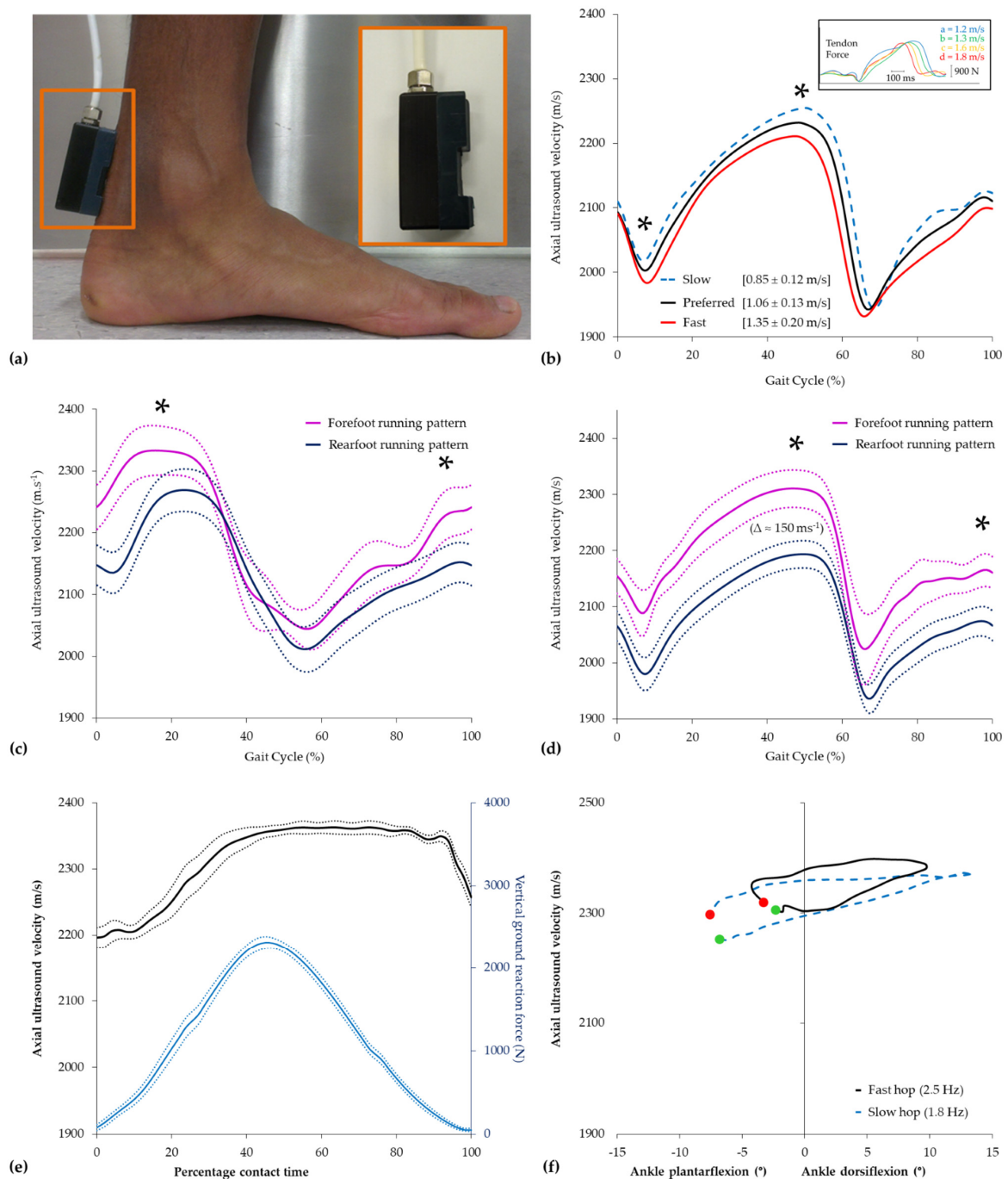
Figure 3. (**a**) Position of the axial-transmission probe over the Achilles tendon. (**b**) Consistent with research employing a direct measure of tensile force in the Achilles tendon (inset), axial velocity of ultrasound in the Achilles tendon is typically biphasic during walking, with peak values systematically reduced with increasing walking speed [173]. (**c**) Foot-strike patterns during running alter the axial velocity of ultrasound in the Achilles tendon [325]. (**d**) The effect of habitual foot-strike patterns on the axial velocity of ultrasound in the Achilles tendon during walking [325]. (**e**) The vertical ground reaction force (blue line) and axial velocity of ultrasound in the Achilles tendon (black line) during a 30-s hopping task [174]. (**f**) The effect of hopping at frequencies of 1.8 Hz (dashed line) and 2.5 Hz (solid line) on ankle movement and the axial velocity of ultrasound in the Achilles tendon [174]. The beginning of contact is denoted by a green circle (•), while the end of contact is denoted by a red circle (•). Note that the dotted lines represent standard deviations. The asterisks indicate a statistically significant difference (*p* < 0.05).

Hopping is a common activity, which is often used clinically to book-end progressive loading programs of the Achilles tendon during functional rehabilitation [327]. Direct measurements of physiological loading in the Achilles tendon have indicated that sub-maximal hopping places greater demands on the Achilles tendon than walking or running [74,75]. Research employing indirect estimates of tendon loading, in contrast, has suggested that Achilles tendon loads during bilateral submaximal hopping are akin to those of running [327]. To the best of the authors' knowledge, only one study to date has applied transmission-mode ultrasound to quantify the change in Achilles tendon properties during hopping. Given that previous research has shown that the major determinant of leg stiffness during hopping switches from knee stiffness to ankle stiffness at a hopping frequency above 2.2 Hz [328–330], our laboratory recorded axial ultrasound velocity in the Achilles tendon of healthy adults while hopping at frequencies above (2.5 Hz) and below (1.8 Hz) this threshold [174]. At each frequency, ultrasound velocity profiles in the Achilles tendon were highly reproducible between cycles, with a mean within-subject coefficient of variation of <1% over the entire ground contact phase, and characterized by a single local minimum and maximum during the contact phase of steady-state hopping (Figure 3e). Maximum and minimum ultrasound velocities recorded in the Achilles tendon during steady-state hopping increased correspondingly with hopping speed (Figure 3f) and were approximately 200 m/s higher than those previously reported in healthy adults during walking at a preferred speed [148,172,320].

Although the peak axial ultrasound velocity in the tendon increased when hopping at the higher frequency, reflecting greater energy storage within the tendon, there was negligible change in the area of the hysteretic loop of the ultrasound-velocity–ankle-angle curve, a surrogate measure of energy loss of the tendon (Figure 3f). The results are thus consistent with *ex vivo* studies of tendon biomechanics in which viscous loss is known to be reduced in tendons exposed to higher strain rates [331]. Moreover, ultrasound velocity profiles in the Achilles tendon during hopping were found to be closely correlated with knee flexion (r = 0.95–1.00) rather than ankle movement (r = 0.35–0.79), highlighting the importance of knee movement to tendon loading and the challenge associated with the deconvolution of the contribution of agonist and antagonist muscles to the net joint moment, especially of bi-articular muscles encountered by inverse dynamic approaches [174].

Finally, axial-transmission ultrasound has also been used to measure *in vivo* properties and loading of the patellar tendon in adults during squatting, a common activity of daily living and exercise used in the rehabilitation of patellar tendinopathy. Axial ultrasound velocity in the patellar tendon was observed to increase non-linearly with knee flexion during the sit-to-stand movement in healthy adults; suggesting an increase in tension within the tendon, which peaked at around 15° of knee flexion [316] (Figure 4). Beyond approximately 20° of flexion, however, the ultrasound velocity within the patellar tendon remained relatively constant. The pattern of loading was highly reproducible (<3% within-subject coefficient of variation) but differed from that reported by previous research, in which inverse dynamics were used to estimate tension in the patellar tendon during squatting and peak force was estimated to occur beyond 80° of flexion [332]. However, the ultrasound velocity pattern in the patellar tendon was consistent with those of cadaveric research in which direct measurements of tendon loading showed that knee flexion beyond approximately 15° progressively lowered tension in the patellar tendon by as much as 50%, relative to that applied to the quadriceps tendon [333].
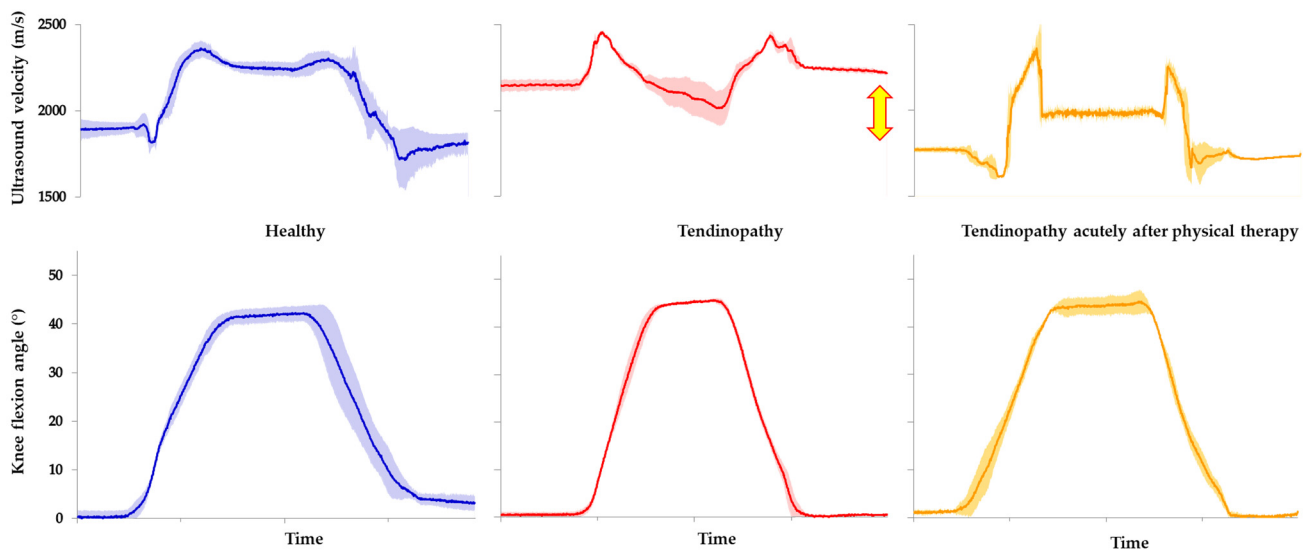
Figure 4. Ensemble axial ultrasound velocity traces in the patellar tendon (**upper panels**) and knee flexion (**lower traces**) during a squat movement in a healthy adult (**left panel**) and in an adult with unilateral patellar tendinopathy prior to (**middle panel**) [316] and immediately following a therapeutic intervention involving manual therapy (**right panel**). To aid in the comparison, traces are time normalized. Shading represents standard deviations determined over three movement cycles. Note the normalization of resting ultrasound velocity values in the painful tendon immediately after therapy (arrow).

4.3.2. Biomechanics of Injured Tendon

Tendon disease represents a spectrum of disorders ranging from reactive tendinopathy, through chronic tendinopathy, to rupture [334]. The most common clinical condition, chronic tendinopathy, is characterized by an underlying state of tissue degeneration [335,336], and is generally thought to reflect an "overuse" injury in which the tendon fails to adapt to prevailing loading conditions [337]. Ultimately, degenerative change associated with prolonged tendinopathy is thought to result in acute tendon rupture in selected cases, which often results in disability and long-term functional limitations [338].

To study the biomechanics of tendon injury, we used transmission-mode ultrasound to measure the *in vivo* loading of the patellar tendon in adults with and without unilateral tendinopathy during squatting [316]. Ultrasound velocity in the patellar tendon differed in young adults with and without chronic unilateral patellar tendinopathy (Figure 4). Despite tendinopathy involving only one tendon, ultrasound velocity was significantly higher (+250 m/s) in the tendons of both the symptomatic and asymptomatic limbs compared to that of healthy adults. The difference in velocity between groups was substantial, mirroring the magnitude of change reported in the equine tendon following surgery [326,339]. Moreover, the results were unexpected in two aspects. First, ultrasound velocity was higher bilaterally in injured adults despite the presence of only unilateral disease. We had hypothesized that ultrasound velocity would be lower in the involved tendon in tendinopathy, reflecting the disorganized collagen structure [335] and the inherently lower intrinsic elastic modulus of the tendon, as shown in previous studies in which an inverse dynamic approach was used to estimate patellar tendon stiffness in tendinopathy [340]. Second, ultrasound velocity was heightened in the tendon but only during a quiet bipedal stance both prior to and following the squat but not during the squat movement. We reasoned that if adults with tendinopathy possessed intrinsically stiffer tendons, which would account for a bilateral increase in ultrasound velocity, the axial velocity would be heightened throughout the entire movement, which was not the case. We concluded, therefore, that resting muscle tone may be increased in both asymptomatic and symptomatic tendons in patellar tendinopathy, resulting in greater loading and, hence, a higher ultrasonic velocity, bilaterally, while at

rest [316]. Indeed, our findings were consistent with the so-called 'vicious cycle' pain theory and with previous research in which the electromyographic activity of agonist muscles is often higher in tendinopathy than in healthy controls [341]. Unpublished data from our laboratory have also highlighted the potential for axial-transmission methods to be used within clinical settings to monitor the effects of therapeutic interventions on the acute loading environment of the tendon (Figure 4).

Our laboratory has also used axial-transmission ultrasound to quantify the recovery state of rupture-repaired tendons. In a cross-sectional study of patients that had surgically repaired Achilles tendons, we observed that the axial velocity of ultrasound in rupture-repaired tendons was significantly lower than that of the contralateral limb during walking, despite symmetrical spatiotemporal gait parameters and vertical ground reaction forces between limbs (Figure 5a) [319]. The magnitude of the reduction in the ultrasound ($\approx$175 m/s) was comparable to that previously reported in the equine flexor tendon ($\approx$140 m/s) following the surgical induction of a core tendon lesion [326] and was suggestive of a lower material stiffness of the repaired tendon. The difference was even more pronounced during a hopping task (Figure 5c,d) [174]. We concluded that the lower material stiffness of the repaired tendon would alter the coordination and functional efficiency of the muscle–tendon unit, which may, in part, underpin reported tendon lengthening and long-term deficits in muscle strength following rupture repair [342,343]. Indeed, neuro-mechanical adaptations, consistent with our findings, have since been reported in subsequent research focused on chronic Achilles tendinopathy, the prequel state to rupture [344]. In contrast to hopping, we also observed no significant difference in the change in ultrasound velocity in repaired and contralateral tendons over a gait cycle. It is noteworthy, however, that the change in ultrasound velocity in the tendon during walking was strongly correlated with self-reported pain and physical function ($r^2 = 0.85$, $p < 0.01$), as defined by the Achilles tendon Rupture Scale [345]. Unpublished data from our laboratory have also highlighted the potential for axial-transmission techniques to be used clinically to monitor the post-operative recovery of tendons following rupture. Figure 5b provides an illustrative example of recovery in the peak axial velocity of ultrasound in a surgically repaired Achilles tendon over a 3-year period following surgery in a male adult while walking on a treadmill at a fixed speed (2.0 m/s). Note that although the peak axial velocity in the rupture-repaired tendon increased exponentially throughout the post-operative period, to approach the lower 95% tolerance interval (with 95% confidence) of the healthy tendon (shaded area), it did not reach the peak axial velocity recorded in the contralateral tendon, which remained relatively unchanged over the 3-year post-operative period. Hence, transmission-mode ultrasound may have the potential to individually guide rehabilitation programs.

When considered collectively, these studies also highlight, for the first time, that different muscle–tendon units may respond differently to a tendon injury, resulting in either an increase or a decrease in tendon loading. Although neuromuscular mechanisms underpinning such a differential response are ongoing, from an applied perspective, such differences have important implications for tendon rehabilitation, in which progressive loading during activities of daily living remains the mainstay of treatment [327,346].
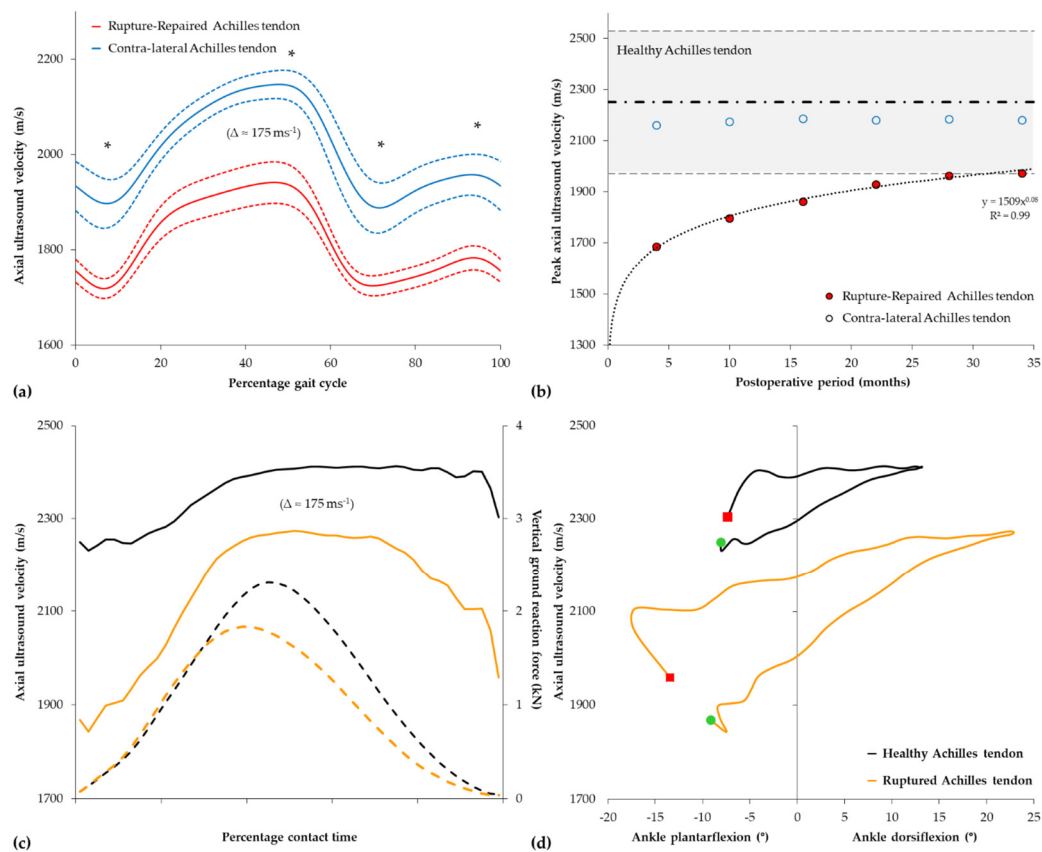
Figure 5. (**a**) Ensemble transmission speed of ultrasound profiles in surgically repaired (red) and contralateral (blue) Achilles tendons during barefoot treadmill walking at 1.05 m/s. Rupture-repaired tendons (n = 10) were characterized by a lower ultrasound velocity at all stages of the gait cycle [319]. The asterisks indicate a statistically significant difference ($p < 0.05$). The dotted lines represent standard deviations. (**b**) Repeated measurements of peak axial ultrasound velocity in the rupture-repaired (●: filled circle) and contralateral (○: empty circle) Achilles tendon of an adult male walking at a fixed speed (2.0 m/s), recorded at 6-month intervals over a 3-year post-operative period. Mean (dash–dot line) and 95% tolerance interval with 95% confidence (gray shaded area) for measurements of peak axial ultrasound velocity recorded in healthy adults (n = 50) walking at the same speed. Note the exponential recovery in the rupture-repaired tendon. (**c**) Axial ultrasound velocity (solid lines) and ground reaction force (dashed lines) profiles in surgically repaired (orange) and healthy (black) Achilles tendons during hopping at 150 bpm [174]. (**d**) Axial ultrasound velocity as a function of ankle joint angle in surgically repaired (orange) and healthy (black) Achilles tendons during hopping. The beginning of contact is denoted by a green circle (●), while the end of contact is denoted by a red square (■). Note that rupture-repaired Achilles tendon is characterized by a greater hysteretic loop than a healthy tendon.

4.3.3. Modification of Tendon Biomechanics via External Influences

Footwear remains a prime candidate for the prevention of tendinopathy and is often used as a key therapeutic intervention in Achilles tendon rehabilitation after injury. The inherent heel offset incorporated in traditional running shoes is thought to elevate the heel and shorten the muscle–tendon unit, thereby decreasing the load in the Achilles tendon during gait [347]. However, supporting evidence for such an effect is equivocal, with elevation of the heel in the order of 15 to 18 mm reported to either increase [348], decrease [349], or have no effect [350,351] on peak tensile loading of the Achilles tendon during running. In a series of repeated-measures studies, in which axial-transmission-mode ultrasound was used to monitor Achilles tendon biomechanics, our laboratory demonstrated that conventional running shoes that incorporated a 10-mm heel offset

(elevation) significantly increased the peak axial velocity of ultrasound and hence, loading in the Achilles tendon during walking [320]. We later demonstrated that a simple orthotic heel lift (22-mm heel offset) may moderate the increase in loading to some extent [321] and that incorporation of a progressive increase in heel offset within the shoe (0 mm–15 mm) resulted in a linear reduction in the peak axial velocity of ultrasound in the tendon during walking [322]. However, we also observed that a substantial manipulation of footwear components, including heel offset, would be required to return the loading environment of the Achilles tendon to that of the barefoot gait [322]. More recently, we also applied this technique to demonstrate that the energy loss properties of shoes also alter the Achilles tendon loading during walking and may be manipulated to either increase energy storage within or reduce energy returned by the tendon [323].

4.4. Measurement of Skeletal Muscle

Quantitative ultrasound was first used *ex vivo* as early as 1982 to characterize the longitudinal and transverse changes in tissue stiffness with muscle contraction in animal models [352]. Using through- and pulse-echo transmission approaches (1, 3, and 7 MHz), Tamura and colleagues [352] demonstrated that, although the propagation speed of ultrasound waves in frog skeletal muscle (n = 20, mean ($\pm$SD) = 1610 $\pm$ 50 m/s) was virtually insensitive to passive force development, tetanic-induced isometric contraction resulted in an increase in propagation velocity in the longitudinal direction ($\approx$245 m/s), coupled with a decrease in velocity in the transverse direction ($\approx$283 m/s) [352,353]. Given that striated muscle stiffness has long been purported to reflect the number of active actin and myosin cross-bridges at any given time [354], Hatta et al. [353] used the same approach to argue that changes in axial ultrasound velocity, as surrogate measurements of muscle stiffness, and provided insight into the cross-bridge function in skeletal muscle.

Despite the pioneering work of Tamura and colleagues [352], the application of quantitative ultrasound techniques for the *in vivo* characterization of human skeletal muscle has been surprisingly sparse in comparison to that of the bone and tendon, only appearing within the literature relatively recently [158,355,356]. In contrast to the tendon, in which the axial-transmission technique predominates, research investigating changes in the properties of human skeletal muscle *in vivo* has almost exclusively adopted pulse-echo transmission techniques to measure the transverse velocity of ultrasound. In contrast to pulse-echo approaches used with the bone, measurements in muscles have most commonly employed a reflector, positioned at a known distance from the emitter [158,170,357,358]. While the use of a reflector aids in the accurate estimation of the transmission velocity of ultrasound waves, wavefront travel times have been shown to be highly sensitive to deviations in reflector inclination angles, which are likely unavoidable in clinical settings [359]. Nonetheless, the technique has been shown to be sufficiently sensitive (area under the receiver–operator characteristic curve = 0.94) to detect differences in the properties of the triceps surae muscles of young (mean ($\pm$SD) age: 28.1 $\pm$ 3.9 years) and elderly adults (82.7 $\pm$ 7 years), with the mean ($\pm$SD) transverse ultrasound velocity in young adults (1550 $\pm$ 8 m/s) reported to be significantly higher than that of the elderly adults (1523 $\pm$ 16 m/s) [158]. Clinical studies have also shown that, in comparison to ultrasound-based measurements of muscle thickness and echotexture, the technique was able to detect changes in skeletal muscle properties with short-term (7 days to 2 months) immobilization, with the transverse ultrasound velocity of the triceps surae muscle being significantly lower than that of the contralateral limb following immobilization [360]. Lower transverse ultrasound velocity, in turn, reportedly correlates moderately to the fat content of the muscle, as determined by the Dixon MRI fat fraction [361]. Consistent with measurements of through-transmission velocity in animal muscle [362], however, quantitative pulse-echo measurements of transverse ultrasound velocity in the muscle are reported to be relatively insensitive to the state of muscle contraction, with the isometric loading of the ankle (up to 650 N) shown to have a negligible effect on the ultrasound velocity (<10 m/s) of the calf muscle when measured in the transverse direction [360]. Hence, the pulse-echo technique, as currently used, does

not appear suitable for characterizing the force-generating capacity or contractile quality of skeletal muscle.

The preliminary work from our laboratory suggests that axial-transmission techniques have the potential to provide suitable quantification of the contractile properties of skeletal muscle. Figure 6a demonstrates the measurements of axial-transmission velocity (nominal 1 MHz) recorded over the biceps brachialis muscle during maximum voluntary isometric contraction. Axial ultrasound velocity was monotonically related to the force measured at the wrist during isometric muscle contraction (Figure 6b), with the change in peak axial ultrasound velocity linearly related to force during submaximal and maximal isometric voluntary contractions (Figure 6c). It is noteworthy that, although the relationship was best fit by a linear model for each individual, the slope varied markedly among healthy adults. We also observed that for a given percentage of maximal isometric contraction of the biceps femoris muscle, elderly adults (n = 8 and mean age (±SD): 82.6 ± 6.4 years) demonstrated a greater change in peak axial-transmission velocity from resting values than young adults (n = 8 and mean age (±SD): 26.0 ± 6.5 years) (Figure 6d). Although further research is required, the results highlight, for the first time, the potential of axial-transmission techniques to quantify the contractile quality of skeletal muscle *in vivo*, particularly within the context of aging and age-related sarcopenia.
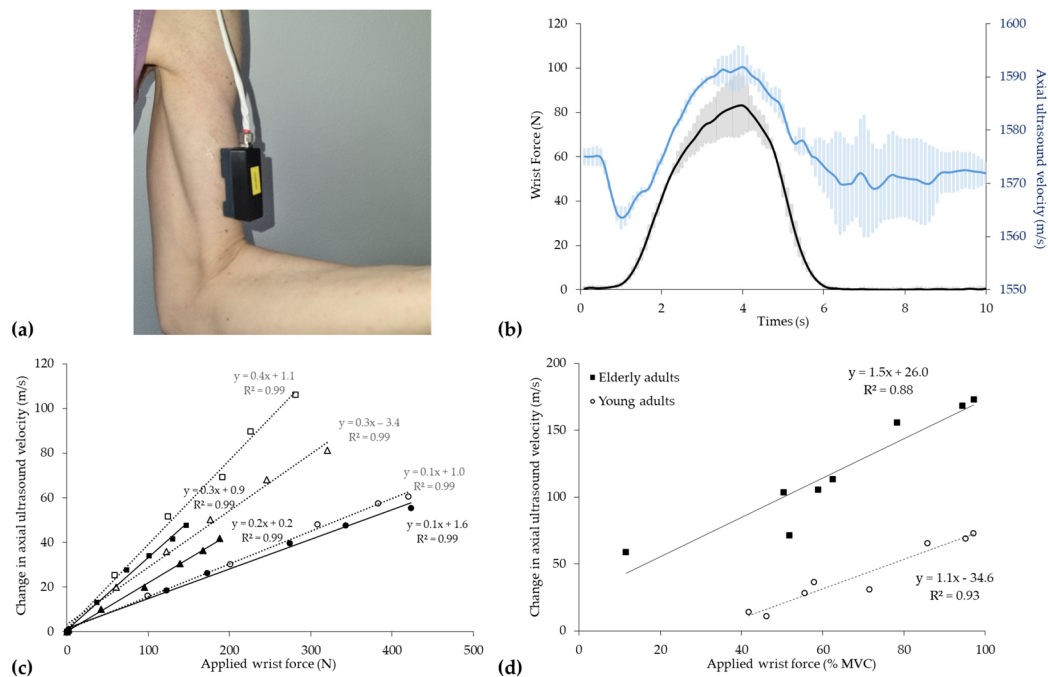
Figure 6. (**a**) Position of the axial-transmission probe (inset) over the belly of the biceps femoris muscle. (**b**) Ensemble force measured at the wrist (N, black line) and axial ultrasound velocity (m/s, blue line) recorded over the biceps femoris muscle during repeated maximum isometric voluntary contractions in a healthy male adult. (**c**) Change in peak axial ultrasound velocity recorded over the biceps femoris muscle in healthy individuals (n = 6) as a function of the force measured at the wrist during submaximal and maximal isometric contractions. Note that for each individual the relationship was best fit by a linear model; however, the slope varied markedly between individuals. (**d**) Change in peak axial ultrasound velocity recorded over the biceps femoris muscle as a function of the force measured at the wrist in young (n = 8 and mean age (±SD): 26.0 ± 6.5 years—empty circle) and elderly adults (n = 8 and mean age (±SD): 82.6 ± 6.4 years—filled square), expressed as a percentage of maximum voluntary isometric contraction. Note that for a given percentage of maximal contraction, elderly adults had a greater change in peak axial-transmission velocity from resting values than young adults.

5. Future Perspectives

For many decades, researchers have worked to advance techniques used for characterizing musculoskeletal tissue properties *in vivo*. Considerable advances in transmission-mode ultrasound techniques have been made since the first *in vivo* application of the through-transmission approach at the calcaneus was detailed in the mid-1980s [142]. Technological developments, coupled with advances in data acquisition and signal processing procedures, have typically been adapted and applied to skeletal structures first, with the translation to soft tissue structures representing the next logical short-term development. Indeed, 3-D multi-frequency and multi-parameter measurements that combine transmission approaches are likely needed for the full characterization of the microstructural and mechanical properties of musculoskeletal tissues [363,364]. To that end, approaches such as ultrasound computed tomography (UCT) have the potential to effectively and efficiently quantify and spatially map human tissue properties in 3D [365,366], albeit at the expense of increased cost and complexity and reduced portability. Current applications have already demonstrated that UCT has the capacity to provide images from various reconstructed acoustic parameters, including the propagation velocity of axial ultrasound waves [367], density, and attenuation [358]. Sequential scanning approaches, such as those used in synthetic transmit aperture (STA) imaging [368], represent a natural extension of current bi-directional transmission approaches [270] and may be a useful adjuvant to aid multi-parameter imaging. Simultaneous developments in wearable ultrasonic arrays are likely to yield viable low-cost methods for extended, serial, and multi-parameter transmission measurements of musculoskeletal tissues that can be acquired at rest during activities of daily living and in settings outside the hospital or the laboratory [369]. Current wearable devices provide 48 h or more of continuous ultrasound scanning to depths of 30–40 mm, with contrast and axial/lateral resolutions in the order of $\approx$3 dB and 0.25/1.0 mm [370]. Such devices have already been applied *in vivo* to monitor skeletal muscle flexion [371] and the change in skeletal muscle modulus following exercise [372]. The future development of these approaches, and in particular, attenuation and backscatter parameters, would undoubtedly benefit from further elucidation of the complex interaction between ultrasound and the microstructures of connective tissues [152,179].

6. Conclusions

The assessment of the biomechanical properties of musculoskeletal tissues has long been recognized as an important tool in the evaluation of tissue adaptation, the early detection and management of pathological conditions, the staging of injury, and the monitoring of the progression of rehabilitation protocols. For this assessment, improving the accurate and non-invasive quantification of the *in vivo* properties of connective tissues in passive states and during activities of daily living remains a significant challenge. Although transmission-mode ultrasound techniques have been applied *in vivo* for the quantification of the structural and mechanical properties of human bone for over 40 years, these techniques have only been introduced relatively recently as non-invasive measurement tools for characterizing muscle and tendon biomechanics *in vivo*. The advancement of the techniques through continuing research will provide opportunities for new insights into the health and disease of musculoskeletal tissues and their biomechanical responses during activities of daily living.

Author Contributions: Conceptualization, C.M.L., N.C.-D., P.P., S.L.H., M.K., T.H. and S.C.W.; writing—original draft preparation, S.C.W.; writing—review and editing, C.M.L., N.C.-D., P.P., S.L.H., M.K. and T.H.; and visualization, S.C.W. All authors have read and agreed to the published version of the manuscript.

Institutional Review Board Statement: Not applicable.

Informed Consent Statement: Not applicable.

References

1. Cieza, A.; Causey, K.; Kamenov, K.; Hanson, S.W.; Chatterji, S.; Vos, T. Global estimates of the need for rehabilitation based on the Global Burden of Disease study 2019: A systematic analysis for the Global Burden of Disease Study 2019. *Lancet* **2021**, *396*, 2006–2017. [CrossRef] [PubMed]

2. Johnell, O.; Kanis, J.A. An estimate of the world-wide prevalence and disability associated with osteoporotic fractures. *Osteoporos. Int.* **2006**, *17*, 1726–1733. [CrossRef] [PubMed]

3. Kanis, J.A.; Norton, N.; Harvey, N.C.; Jacobson, T.; Johansson, H.; Lorentzon, M.; McCloskey, E.V.; Willers, C.; Borgström, F. SCOPE 2021: A new scorecard for osteoporosis in Europe. *Arch. Osteoporos.* **2021**, *16*, 82. [CrossRef] [PubMed]

4. Petermann-Rocha, F.; Balntzi, V.; Gray, S.R.; Lara, J.; Ho, F.K.; Pell, J.P.; Celis-Morales, C. Global prevalence of sarcopenia and severe sarcopenia: A systematic review and meta-analysis. *J. Cachexia Sarcopenia Muscle* **2022**, *13*, 86–99. [CrossRef] [PubMed]

5. McCormick, A.; Charlton, J.; Fleming, D. Assessing health needs in primary care. Morbidity study from general practice provides another source of information. *BMJ* **1995**, *310*, 1534. [CrossRef] [PubMed]

6. Sebbag, E.; Felten, R.; Sagez, F.; Sibilia, J.; DeVilliers, H.; Arnaud, L. The world-wide burden of musculoskeletal diseases: A systematic analysis of the World Health Organization Burden of Diseases Database. *Ann. Rheum. Dis.* **2019**, *78*, 844–848. [CrossRef] [PubMed]

7. GBD 2021 Other Musculoskeletal Disorders Collaborators. Global, regional, and national burden of other musculoskeletal disorders, 1990–2020, and projections to 2050: A system-atic analysis of the Global Burden of Disease Study 2021. *Lancet Rheumatol.* **2023**, *5*, e670–e682. [CrossRef] [PubMed]

8. Guimarães, C.F.; Gasperini, L.; Marques, A.P.; Reis, R.L. The stiffness of living tissues and its implications for tissue engineering. *Nat. Rev. Mater.* **2020**, *5*, 351–370. [CrossRef]

9. Frost, H.M. The mechanostat: A proposed pathogenetic mechanism of osteoporoses and the bone mass effects of mechanical and nonmechanical agents. *Bone Min.* **1987**, *2*, 73–85.

10. Frost, H.M. Perspectives: A proposed general model for the mechanostat (suggestions from a new paradigm). *Anat. Rec.* **1996**, *244*, 139–147. [CrossRef]

11. Frost, H.M. Bone's mechanostat: A 2003 update. *Anat. Rec.* **2003**, *275A*, 1081–1101. [CrossRef] [PubMed]

12. LaMothe, J.M.; Hamilton, N.H.; Zernicke, R.F. Strain rate influences periosteal adaptation in mature bone. *Med. Eng. Phys.* **2005**, *27*, 277–284. [CrossRef] [PubMed]

13. Miller, C.J.; Trichilo, S.; Pickering, E.; Martelli, S.; Delisser, P.; Meakin, L.B.; Pivonka, P. Cortical thickness adaptive response to mechanical loading depends on periosteal position and varies linearly with loading magnitude. *Front. Bioeng. Biotechnol.* **2021**, *9*, 671606. [CrossRef] [PubMed]

14. Wisdom, K.M.; Delp, S.L.; Kuhl, E. Use it or lose it: Multiscale skeletal muscle adaptation to mechanical stimuli. *Biomech. Model. Mechanobiol.* **2015**, *14*, 195–215. [CrossRef] [PubMed]

15. Quinlan, J.I.; Franchi, M.V.; Gharahdaghi, N.; Badiali, F.; Francis, S.; Hale, A.; Phillips, B.E.; Szewczyk, N.; Greenhaff, P.L.; Smith, K.; et al. Muscle and tendon adaptations to moderate load eccentric vs. concentric resistance exercise in young and older males. *GeroScience* **2021**, *43*, 1567–1584. [CrossRef] [PubMed]

16. Bohm, S.; Mersmann, F.; Tettke, M.; Kraft, M.; Arampatzis, A. Human Achilles tendon plasticity in response to cyclic strain: Effect of rate and duration. *J. Exp. Biol.* **2014**, *217*, 4010–4017. [CrossRef] [PubMed]

17. Skerry, T.M. One mechanostat or many? Modifications of the site-specific response of bone to mechanical loading by nature and nurture. *J. Musculoskelet. Neuronal Interact.* **2006**, *6*, 122–127. [PubMed]

18. Kasashima, Y.; Takahashi, T.; Birch, H.L.; Smith, R.K.W.; Goodship, A.E. Can exercise modulate the maturation of functionally different immature tendons in the horse? *J. Appl. Physiol.* **2008**, *104*, 416–422. [CrossRef] [PubMed]

19. Skerry, T.M. The response of bone to mechanical loading and disuse: Fundamental princi-ples and influences on os-teoblast/osteocyte homeostasis. *Arch. Biochem. Biophys.* **2008**, *473*, 117–123. [CrossRef]

20. Louis, O.; Boulpaep, F.; Willnecker, J.; Van-den-Winkel, P.; Osteaux, M. Cortical mineral content of the radius assessed by peripheral QCT predicts compressive strength on biomechanical testing. *Bone* **1995**, *16*, 375–379. [CrossRef] [PubMed]

21. Martin, R.B.; Ishida, J. The relative effects of collagen fiber orientation, porosity, density, and mineralization on bone strength. *J. Biomech.* **1989**, *22*, 419–426. [CrossRef] [PubMed]

22. Wachter, N.J.; Krischak, G.D.; Mentzel, M.; Sarkar, M.R.; Ebinger, T.; Kinzl, L.; Claes, L.; Augat, P. Correlation of bone mineral density with strength and microstructural parameters of cortical bone in vitro. *Bone* **2002**, *31*, 90–95. [CrossRef] [PubMed]

23. Choksi, P.; Jepsen, K.J.; Clines, G.A. The challenges of diagnosing osteoporosis and the limitations of currently available tools. *Clin. Diabetes Endocrinol.* **2018**, *4*, 12. [CrossRef] [PubMed]

24. Bolotin, H.H. DXA *in vivo* BMD methodology: An erroneous and misleading research and clinical gauge of bone mineral status, bone fragility, and bone remodelling. *Bone* **2007**, *41*, 138–154. [CrossRef] [PubMed]

25. Golding, P.H. Dual-energy X-ray absorptiometry (DXA) to measure bone mineral density (BMD) for diagnosis of osteoporosis—Experimental data from artificial vertebrae confirms significant dependence on bone size. *Bone Rep.* **2022**, *17*, 101607. [CrossRef] [PubMed]

26. Kanis, J.A. Diagnosis of osteoporosis and assessment of fracture risk. *Lancet* **2002**, *359*, 1929–1936. [CrossRef] [PubMed]

27. Bala, Y.; Zebaze, R.; Seeman, E. Role of cortical bone in bone fragility. *Curr. Opin. Rheumatol.* **2015**, *27*, 406–413. [CrossRef] [PubMed]

28. Wainwright, S.A.; Marshall, L.M.; Ensrud, K.E.; Cauley, J.A.; Black, D.M.; Hillier, T.A.; Hochberg, M.C.; Vogt, M.T.; Orwoll, E.S.; Study of Osteoporotic Fractures Research Group. Hip fracture in women without osteoporosis. *J. Clin. Endocrinol. Metab.* **2005**, *90*, 2787–2793. [CrossRef] [PubMed]

29. Wang, Y.; Yu, S.; Hsu, C.; Tsai, C.; Cheng, T. Underestimated fracture risk in postmenopausal women-application of the hybrid intervention threshold. *Osteoporos. Int.* **2020**, *31*, 475–483. [CrossRef] [PubMed]

30. Lespessailles, E.; Cortet, B.; Legrand, E.; Guggenbuhl, P.; Roux, C. Low-trauma fractures without osteoporosis. *Osteoporos. Int.* **2017**, *28*, 1771–1778. [CrossRef] [PubMed]

31. Saraff, V.; Hogler, W. Endocrinology and adolescence: Osteoporosis in children: Diagnosis and management. *Eur. J. Endocrinol.* **2015**, *173*, R185–R197. [CrossRef] [PubMed]

32. Zhou, B.; Wang, J.; Yu, Y.E.; Zhang, Z.; Nawathe, S.; Nishiyama, K.K.; Rosete, F.R.; Keaveny, T.M.; Shane, E.; Guo, X.E. High-resolution peripheral quantitative computed tomography (HR-pQCT) can assess microstructural and biomechanical properties of both human distal radius and tibia: *Ex vivo* computational and experimental validations. *Bone* **2016**, *86*, 58–67. [CrossRef] [PubMed]

33. Liu, X.S.; Zhang, X.H.; Sekhon, K.K.; Adams, M.F.; McMahon, D.J.; Bilezikian, J.; Shane, E.; Guo, X.E. High-resolution peripheral quantitative computed tomography can assess microstructural and mechanical properties of human distal tibial bone. *J. Bone Min. Res.* **2010**, *25*, 746–756. [CrossRef] [PubMed]

34. Chiba, K.; Okazaki, N.; Kurogi, A.; Isobe, Y.; Yonekura, A.; Tomita, M.; Osaki, M. Precision of sec-ond-generation high-resolution peripheral quantitative computed tomography: Intra- and intertester reproducibilities and factors involved in the reproducibility of cortical porosity. *J. Clin. Densitom.* **2018**, *21*, 295–302. [CrossRef] [PubMed]

35. Gazzotti, S.; Aparisi Gómez, M.P.; Schileo, E.; Taddei, F.; Sangiorgi, L.; Fusaro, M.; Miceli, M.; Gug-lielmi, G.; Bazzocchi, A. High-resolution peripheral quantitative computed tomography: Research or clinical practice? *Br. J. Radiol.* **2023**, *96*, 20221016. [CrossRef] [PubMed]

36. Lanyon, L.E.; Hampson, W.G.; Goodship, A.E.; Shah, J.S. Bone deformation recorded *in vivo* from strain gauges attached to the human tibial shaft. *Acta Orthop. Scand.* **1975**, *46*, 256–268. [CrossRef] [PubMed]

37. Burr, D.B.; Milgrom, C.; Fyhrie, D.; Forwood, M.; Nyska, M.; Finestone, A.; Hoshaw, S.; Saiag, E.; Simkin, A. *In vivo* measurement of human tibial strains during vigorous activity. *Bone* **1996**, *18*, 405–410. [CrossRef] [PubMed]

38. Kersh, M.E.; Martelli, S.; Zebaze, R.; Seeman, E.; Pandy, M.G. Mechanical loading of the femoral neck in human locomotion. *J. Bone Min. Res.* **2018**, *33*, 1999–2006. [CrossRef] [PubMed]

39. Al Nazer, R.; Lanovaz, J.; Kawalilak, C.; Johnston, J.D.; Kontulainen, S. Direct *in vivo* strain measurements in human bone—A systematic literature review. *J. Biomech.* **2012**, *45*, 27–40. [CrossRef] [PubMed]

40. Konrath, J.M.; Karatsidis, A.; Schepers, H.M.; Bellusci, G.; de Zee, M.; Andersen, M.S. Estimation of the knee adduction moment and joint contact force during daily living activities using inertial motion capture. *Sensors* **2019**, *19*, 1681. [CrossRef] [PubMed]

41. Actis, J.A.; Honegger, J.D.; Gates, D.H.; Petrella, A.J.; Nolasco, L.A.; Silverman, A.K. Validation of lumbar spine loading from a musculoskeletal model including the lower limbs and lumbar spine. *J. Biomech.* **2018**, *68*, 107–114. [CrossRef] [PubMed]

42. Lin, Y.; Walter, J.P.; Pandy, M.G. Predictive simulations of neuromuscular coordination and joint-contact loading in human gait. *Ann. Biomed. Eng.* **2018**, *46*, 1216–1227. [CrossRef] [PubMed]

43. Matijevich, E.S.; Branscombe, L.M.; Scott, L.R.; Zelik, K.E. Ground reaction force metrics are not strongly correlated with tibial bone load when running across speeds and slopes: Implications for science, sport and wearable tech. *PLoS ONE* **2019**, *14*, e0210000. [CrossRef] [PubMed]

44. Cleather, D.J.; Goodwin, J.E.; Bull, A.M. Hip and knee joint loading during vertical jumping and push jerking. *Clin. Biomech.* **2013**, *28*, 98–103. [CrossRef] [PubMed]

45. Zdero, R.; Brzozowski, P.; Schemitsch, E.H. Experimental methods for studying the contact mechanics of joints. *Biomed. Res. Int.* **2023**, *2023*, 4914082. [CrossRef] [PubMed]

46. Currey, J.D. The structure and mechanics of bone. *J. Mater. Sci.* **2012**, *47*, 41–54. [CrossRef]

47. Fregly, B.J.; Besier, T.F.; Lloyd, D.G.; Delp, S.L.; Banks, S.A.; Pandy, M.G.; D'Lima, D.D. Grand challenge competition to predict *in vivo* knee loads. *J. Orthop. Res.* **2012**, *30*, 503–513. [CrossRef] [PubMed]

48. Bergmann, G.; Deuretzbacher, G.; Heller, M.; Graichen, F.; Rohlmann, A.; Strauss, J.; Duda, G.N. Hip contact forces and gait patterns from routine activities. *J. Biomech.* **2001**, *34*, 859–871. [CrossRef] [PubMed]

49. Kinney, A.L.; Besier, T.F.; D'Lima, D.D.; Fregly, B.J. Update on grand challenge competition to predict *in vivo* knee loads. *J. Biomech. Eng.* **2013**, *135*, 021012. [CrossRef] [PubMed]

50. Ding, Z.; Nolte, D.; Kit Tsang, C.; Cleather, D.J.; Kedgley, A.E.; Bull, A.M. *In vivo* knee contact force prediction using patient-specific musculoskeletal geometry in a segment-based computational model. *J. Biomech. Eng.* **2016**, *138*, 021018. [CrossRef] [PubMed]

51. Jung, Y.; Phan, C.-B.; Koo, S. Intra-articular knee contact force estimation during walking using force-reaction elements and subject-specific joint model. *J. Biomech. Eng.* **2016**, *138*, 021016. [CrossRef] [PubMed]

52. Amiri, P.; Bull, A.M.J. Prediction of *in vivo* hip contact forces during common activities of daily living using a segment-based musculoskeletal model. *Front. Bioeng. Biotechnol.* **2022**, *10*, 995279. [CrossRef] [PubMed]

53. Moissenet, F.; Modenese, L.; Dumas, R. Alterations of musculoskeletal models for a more accurate estimation of lower limb joint contact forces during normal gait: A systematic review. *J. Biomech.* **2017**, *63*, 8–20. [CrossRef] [PubMed]

54. Schellenberg, F.; Taylor, W.R.; Trepczynski, A.; List, R.; Kutzner, I.; Schutz, P.; Duda, G.N.; Lorenzetti, S. Evaluation of the accuracy of musculoskeletal simulation during squats by means of instrumented knee prostheses. *Med. Eng. Phys.* **2018**, *61*, 95–99. [CrossRef] [PubMed]

55. Trepczynski, A.; Kutzner, I.; Kornaropoulos, E.; Taylor, W.R.; Duda, G.N.; Bergmann, G.; Heller, M.O. Patellofemoral joint contact forces during activities with high knee flexion. *J. Orthop. Res.* **2012**, *30*, 408–415. [CrossRef] [PubMed]

56. Martin, J.A.; Brandon, S.C.E.; Keuler, E.M.; Hermus, J.R.; Ehlers, A.C.; Segalman, D.J.; Allen, M.S.; Thelen, D.G. Gauging force by tapping tendons. *Nat. Commun.* **2018**, *9*, 1592. [CrossRef] [PubMed]

57. Salman, M.; Sabra, K.G. Assessing non-uniform stiffening of the achilles tendon noninvasively using surface wave. *J. Biomech.* **2019**, *82*, 357–360. [CrossRef] [PubMed]

58. Keuler, E.M.; Loegering, I.F.; Martin, J.A.; Roth, J.D.; Thelen, D.G. Shear wave predictions of Achilles tendon loading during human walking. *Sci. Rep.* **2019**, *9*, 13419. [CrossRef] [PubMed]

59. Obuchowicz, R.; Ambrozinski, L.; Kohut, P. Influence of load and transducer bandwidth on the repeatability of *in vivo* tendon stiffness evaluation using shear wave elastography. *J. Diagn. Med. Sonogr.* **2020**, *36*, 409–420. [CrossRef]

60. Maganaris, C.N.; Paul, J.P. *In vivo* human tendon mechanical properties. *J. Physiol.* **1999**, *521*, 307–313. [CrossRef] [PubMed]

61. Kárason, H.; Ritrovato, P.; Maffulli, N.; Boccaccini, A.R.; Tortorella, F. Wearable approaches for non-invasive monitoring of tendons: A scoping review. *Internet Things* **2024**, *26*, 101199. [CrossRef]

62. Arampatzis, A.; Karamanidis, K.; Albracht, K. Adaptational responses of the human Achilles tendon by modulation of the applied cyclic strain magnitude. *J. Exp. Biol.* **2007**, *210*, 2743–2753. [CrossRef] [PubMed]

63. Arampatzis, A.; Peper, A.; Bierbaum, S.; Albracht, K. Plasticity of human Achilles tendon mechanical and morphological properties in response to cyclic strain. *J. Biomech.* **2010**, *43*, 3073–3079. [CrossRef] [PubMed]

64. Seynnes, O.R.; Bojsen-Møller, J.; Albracht, K.; Arndt, A.; Cronin, N.J.; Finni, T.; Magnusson, S.P. Ultrasound-based testing of tendon mechanical properties: A critical evaluation. *J. Appl. Physiol.* **2015**, *118*, 133–141. [CrossRef] [PubMed]

65. Gregor, R.J.; Komi, P.V.; Browning, R.C.; Järvinen, M. A comparison of the triceps surae and residual muscle moments at the ankle during cycling. *J. Biomech.* **1991**, *24*, 287–297. [CrossRef] [PubMed]

66. Fukashiro, S.; Komi, P.; Järvinen, M.; Miyashita, M. Comparison between the directly measured achilles tendon force and the tendon force calculated from the ankle joint moment during vertical jumps. *Clin. Biomech.* **1993**, *8*, 25–30. [CrossRef] [PubMed]

67. Zelik, K.E.; Franz, J.R. It's positive to be negative: Achilles tendon work loops during human locomotion. *PLoS ONE* **2017**, *12*, e0179976. [CrossRef] [PubMed]

68. Ravary, B.; Pourcelot, P.; Bortolussi, C.; Konieczka, S.; Crevier-Denoix, N. Strain and force transducers used in human and veterinary tendon and ligament biome-chanical studies. *Clin. Biomech.* **2004**, *19*, 433–447. [CrossRef] [PubMed]

69. Finni, T.; Komi, P.V.; Lukkariniemi, J. Achilles tendon loading during walking: Application of a novel optic fiber technique. *Eur. J. Appl. Physiol. Occup. Physiol.* **1998**, *77*, 289–291. [CrossRef] [PubMed]

70. Finni, T.; Komi, P.V.; Lepola, V. *In vivo* human triceps surae and quadriceps femoris muscle function in a squat jump and counter movement jump. *Eur. J. Appl. Physiol.* **2000**, *83*, 416–426. [CrossRef] [PubMed]

71. Gregor, R.J.; Komi, P.V.; Järvinen, M. Achilles tendon forces during cycling. *Int. J. Sports Med.* **1987**, *8*, 9–14. [CrossRef] [PubMed]

72. Komi, P.V. Relevance of *in vivo* force measurements to human biomechanics. *J. Biomech.* **1990**, *23*, 23–34. [CrossRef] [PubMed]

73. Kyröläinen, H.; Finni, T.; Avela, J.; Komi, P.V. Neuromuscular behaviour of the triceps surae muscle-tendon complex during running and jumping. *Int. J. Sports Med.* **2003**, *24*, 153–155. [CrossRef] [PubMed]

74. Fukashiro, S.; Komi, P.V.; Järvinen, M.; Miyashita, M. *In vivo* Achilles tendon loading during jumping in humans. *Eur. J. Appl. Physiol. Occup. Physiol.* **1995**, *71*, 453–458. [CrossRef] [PubMed]

75. Komi, P.V.; Fukashiro, S.; Järvinen, M. Biomechanical loading of Achilles tendon during normal locomotion. *Clin. Sports Med.* **1992**, *11*, 521–531. [CrossRef] [PubMed]

76. Kursa, K.; Lattanza, L.; Diao, E.; Rempel, D. *In vivo* flexor tendon forces increase with finger and wrist flexion during active finger flexion and extension. *J. Orthop. Res.* **2006**, *24*, 763–769. [CrossRef] [PubMed]

77. Lewis, J.L.; Lew, W.D.; Schmidt, J. A note on the application and evaluation of the buckle transducer for knee ligament force measurement. *J. Biomech. Eng.* **1982**, *104*, 125–128. [CrossRef] [PubMed]

78. Gennisson, J.-L.; Deffieux, T.; Fink, M.; Tanter, M. Ultrasound elastography: Principles and techniques. *Diagn. Interv. Imaging* **2013**, *94*, 487–495. [CrossRef] [PubMed]

79. Shiina, T.; Nightingale, K.R.; Palmeri, M.L.; Hall, T.J.; Bamber, J.C.; Barr, R.G.; Castera, L.; Choi, B.I.; Chou, Y.H.; Cosgrove, D.; et al. WFUMB guide-lines and recommendations for clinical use of ultrasound elastography: Part 1: Basic principles and terminology. *Ultrasound Med. Biol.* **2015**, *41*, 1126–1147. [CrossRef] [PubMed]

80. Bamber, J.; Cosgrove, D.; Dietrich, C.F.; Fromageau, J.; Bojunga, J.; Calliada, F.; Cantisani, V.; Correas, J.-M.; D'Onofrio, M.; Drakonaki, E.E.; et al. EFSUMB guidelines and recommendations on the clinical use of ultrasound elastography. Part 1: Basic principles and technology. *Ultraschall Med.* **2013**, *34*, 169–184. [CrossRef] [PubMed]

81. Sigrist, R.M.S.; Liau, J.; Kaffas, A.E.; Chammas, M.C.; Willmann, J.K. Ultrasound elastography: Review of techniques and clinical applications. *Theranostics* **2017**, *7*, 1303–1329. [CrossRef] [PubMed]

82. Youk, J.H.; Gweon, H.M.; Son, E.J. Shear-wave elastography in breast ultrasonography: The state of the art. *Ultrasonography* **2017**, *36*, 300–309. [CrossRef] [PubMed]

83. Taljanovic, M.S.; Gimber, L.H.; Becker, G.W.; Latt, L.D.; Klauser, A.S.; Melville, D.M.; Gao, L.; Witte, R.S. Shear-wave elastography: Basic physics and musculoskeletal applications. *Radiographics* **2017**, *37*, 855–870. [CrossRef]

84. Chiu, Y.H.; Chang, K.V.; Chen, I.J.; Wu, W.T.; Özçakar, L. Utility of sonoelastography for the evaluation of rotator cuff tendon and pertinent disorders: A systematic review and meta-analysis. *Eur. Radiol.* **2020**, *30*, 6663–6672. [CrossRef] [PubMed]

85. Lin, C.P.; Chen, I.J.; Chang, K.V.; Wu, W.T.; Özçakar, L. Utility of ultrasound elastography in evaluation of carpal tunnel syndrome: A systematic review and meta-analysis. *Ultrasound Med. Biol.* **2019**, *45*, 2855–2865. [CrossRef]

86. Maganaris, C.N. Tensile properties of *in vivo* human tendinous tissue. *J. Biomech.* **2002**, *35*, 1019–1027. [CrossRef]

87. Pollock, C.M.; Shadwick, R.E. Relationship between body mass and biomechanical properties of limb tendons in adult mammals. *Am. J. Physiol.* **1994**, *266*, R1016–R1021. [CrossRef] [PubMed]

88. Götschi, T.; Schulz, N.; Snedeker, J.G.; Hanimann, J.; Franchi, M.V.; Spörri, J. Three-dimensional mapping of shear wave velocity in human tendon: A proof of concept study. *Sensors* **2021**, *21*, 1655. [CrossRef] [PubMed]

89. Pelivanov, I.; Gao, L.; Pitre, J.; Kirby, M.A.; Song, S.; Li, D.; Shen, T.T.; Wang, R.K.; O'Donnell, M. Does group velocity always reflect elastic modulus in shear wave elastography? *J. Biomed. Opt.* **2019**, *24*, 1. [CrossRef] [PubMed]

90. Royer, D.; Gennisson, J.-L.; Deffieux, T.; Tanter, M. On the elasticity of transverse isotropic soft tissues (L). *J. Acoust. Soc. Am.* **2011**, *129*, 2757–2760. [CrossRef] [PubMed]

91. Glozman, T.; Azhari, H. A method for characterization of tissue elastic properties combining ultrasonic computed tomography with elastography. *J. Ultrasound Med.* **2010**, *29*, 387–398. [CrossRef] [PubMed]

92. Martin, J.A.; Biedrzycki, A.H.; Lee, K.S.; DeWall, R.J.; Brounts, S.H.; Murphy, W.L.; Markel, M.D.; Thelen, D.G. *In vivo* measures of shear wave speed as a predictor of tendon elasticity and strength. *Ultrasound Med. Biol.* **2015**, *41*, 2722–2730. [CrossRef] [PubMed]

93. Mifsud, T.; Chatzistergos, P.; Maganaris, C.; Chockalingam, N.; Padhiar, N.; Micallef Stafrace, K.; Gatt, A. Supersonic shear wave elastography of human tendons is associated with *in vivo* tendon stiffness over small strains. *J. Biomech.* **2023**, *152*, 111558. [CrossRef] [PubMed]

94. Götschi, T.; Schärer, Y.; Gennisson, J.L.; Snedeker, J.G. Investigation of the relationship between tensile viscoelasticity and unloaded ultrasound shear wave measurements in *ex vivo* tendon. *J. Biomech.* **2023**, *146*, 111411. [CrossRef] [PubMed]

95. Rominger, M.B.; Kälin, P.; Mastalerz, M.; Martini, K.; Klingmüller, V.; Sanabria, S.; Frauenfelder, T. Influencing factors of 2d shear wave elastography of the muscle—An *ex vivo* animal study. *Ultrasound Int. Open* **2018**, *4*, E54–E60. [CrossRef] [PubMed]

96. Ruby, L.; Mutschler, T.; Martini, K.; Klingmüller, V.; Frauenfelder, T.; Rominger, M.B.; Sanabria, S.J. Which confounders have the largest impact in shear wave elastography of muscle and how can they be minimized? an elasticity phantom, *ex vivo* porcine muscle and volunteer study using a commercially available system. *Ultrasound Med. Biol.* **2019**, *45*, 2591–2611. [CrossRef] [PubMed]

97. Šarabon, N.; Kozinc, Ž.; Podrekar, N. Using shear-wave elastography in skeletal muscle: A repeatability and reproducibility study on biceps femoris muscle. *PLoS ONE* **2019**, *14*, e0222008. [CrossRef] [PubMed]

98. Fielding, R.A.; Vellas, B.; Evans, W.J.; Bhasin, S.; Morley, J.E.; Newman, A.B.; Abellan van Kan, G.; Andrieu, S.; Bauer, J.; Breuille, D.; et al. Sarcopenia: An undiagnosed condition in older adults. Current consensus definition: Prevalence, etiology, and consequences. International working group on sarcopenia. *J. Am. Med. Dir. Assoc.* **2011**, *12*, 249–256. [CrossRef] [PubMed]

99. Cruz-Jentoft, A.J.; Bahat, G.; Bauer, J.; Boirie, Y.; Bruyère, O.; Cederholm, T.; Cooper, C.; Landi, F.; Rolland, Y.; Sayer, A.A.; et al. Sarcopenia: Revised European consensus on definition and diagnosis. *Age Ageing* **2019**, *48*, 16–31. [CrossRef] [PubMed]

100. Abdalla, P.P.; da Silva, L.S.L.; Venturini, A.C.R.; Júnior, M.F.T.; Schneider, G.; Dos Santos, A.P.; Gomide, E.B.G.; Carvalho, A.D.S.; Bohn, L. Anthropometric equations to estimate appendicular muscle mass from dual-energy X-ray absorptiometry (DXA): A scoping review. *Arch. Gerontol. Geriatr.* **2023**, *110*, 104972. [CrossRef] [PubMed]

101. Pietrobelli, A.; Morini, P.; Battistini, N.; Chiumello, G.; Nuñez, C.; Heymsfield, S.B. Appendicular skeletal muscle mass: Prediction from multiple frequency segmental bioimpedance analysis. *Eur. J. Clin. Nutr.* **1998**, *52*, 507–511. [CrossRef] [PubMed]

102. McCarthy, C.; Tinsley, G.M.; Bosy-Westphal, A.; Müller, M.J.; Shepherd, J.; Gallagher, D.; Heymsfield, S.B. Total and regional appendicular skeletal muscle mass prediction from dual-energy X-ray absorptiometry body composition models. *Sci. Rep.* **2023**, *13*, 2590. [CrossRef] [PubMed]

103. Varol, U.; Sánchez-Jiménez, E.; Leloup, E.A.A.; Navarro-Santana, M.J.; Fernández-de-Las-Peñas, C.; Sánchez-Jorge, S.; Valera-Calero, J.A. Correlation between body composition and inter-examiner errors for assessing lumbar multifidus muscle size, shape and quality metrics with ultrasound imaging. *Bioengineering* **2023**, *10*, 133. [CrossRef] [PubMed]

104. Emanuelsson, E.B.; Berry, D.B.; Reitzner, S.M.; Arif, M.; Mardinoglu, A.; Gustafsson, T.; Ward, S.R.; Sundberg, C.J.; Chapman, M.A. MRI characterization of skeletal muscle size and fatty infiltration in long-term trained and untrained individuals. *Physiol. Rep.* **2022**, *10*, e15398. [CrossRef] [PubMed]

105. Verdijk, L.B.; Gleeson, B.G.; Jonkers, R.A.; Meijer, K.; Savelberg, H.H.; Dendale, P.; van Loon, L.J.C. Skeletal muscle hypertrophy following resistance training is accompanied by a fiber type-specific increase in satellite cell content in elderly men. *J. Gerontol. A Biol. Sci. Med. Sci.* **2009**, *64*, 332–339. [CrossRef] [PubMed]

106. DeFreitas, J.M.; Beck, T.W.; Stock, M.S.; Dillon, M.A.; Sherk, V.D.; Stout, J.R.; Cramer, J.T. A comparison of techniques for estimating training-induced changes in muscle cross-sectional area. *J. Strength. Cond. Res.* **2010**, *24*, 2383–2389. [CrossRef] [PubMed]

107. Di Sebastiano, K.M.; Mourtzakis, M. A critical evaluation of body composition modalities used to assess adipose and skeletal muscle tissue in cancer. *Appl. Physiol. Nutr. Metab.* **2012**, *37*, 811–821. [CrossRef] [PubMed]

108. Bilston, L.E.; Bolsterlee, B.; Nordez, A.; Sinha, S. Contemporary image-based methods for measuring passive mechanical properties of skeletal muscles *in vivo*. *J. Appl. Physiol.* **2019**, *126*, 1454–1464. [CrossRef] [PubMed]

109. Walowski, C.O.; Braun, W.; Maisch, M.J.; Jensen, B.; Peine, S.; Norman, K.; Müller, M.J.; Bosy-Westphal, A. Reference values for skeletal muscle mass—Current concepts and methodological considerations. *Nutrients* **2020**, *12*, 755. [CrossRef] [PubMed]

110. Naimo, M.A.; Varanoske, A.N.; Hughes, J.M.; Pasiakos, S.M. Skeletal muscle quality: A biomarker for assessing physical performance capabilities in young populations. *Front. Physiol.* **2021**, *12*, 706699. [CrossRef] [PubMed]

111. Engelke, K.; Museyko, O.; Wang, L.; Laredod, J.-D. Quantitative anal-ysis of skeletal muscle by computed tomography imaging—State of the art. *J. Orthop. Transl.* **2018**, *15*, 91–103. [CrossRef]

112. Faron, A.; Sprinkart, A.M.; Kuetting, D.L.R.; Feisst, A.; Isaak, A.; Endler, C.; Chang, J.; Nowak, S.; Block, W.; Thomas, D.; et al. Body composition analysis using CT and MRI: Intra-individual intermodal comparison of muscle mass and myosteatosis. *Sci. Rep.* **2020**, *10*, 11765. [CrossRef] [PubMed]

113. van der Werf, A.; Langius, J.A.E.; de van der Schueren, M.A.E.; Nurmohamed, S.A.; van der Pant, K.A.M.I.; Blauwhoff-Buskermolen, S.; Wierdsma, V.J. Percentiles for skeletal muscle index, area and radiation attenuation based on computed tomography imaging in a healthy Caucasian population. *Eur. J. Clin. Nutr.* **2018**, *72*, 288–296. [CrossRef] [PubMed]

114. Li, G.D.; Liang, Y.Y.; Xu, P.; Ling, J.; Chen, Y.M. Diffusion-tensor imaging of thigh muscles in Duchenne muscular dystrophy: Correlation of apparent diffusion coefficient and fractional anisotropy values with fatty infiltration. *Am. J. Roentgenol.* **2016**, *206*, 867–870. [CrossRef] [PubMed]

115. Bilston, L.E.; Tan, K. Measurement of passive skeletal muscle mechanical properties *in vivo*: Recent progress, clinical applications, and remaining challenges. *Ann. Biomed. Eng.* **2015**, *43*, 261–273. [CrossRef]

116. Jenkyn, T.R.; Ehman, R.L.; An, K.N. Noninvasive muscle tension measurement using the novel technique of magnetic resonance elastography (MRE). *J. Biomech.* **2003**, *36*, 1917–1921. [CrossRef] [PubMed]

117. Ringleb, S.I.; Bensamoun, S.F.; Chen, Q.; Manduca, A.; An, K.N.; Ehman, R.L. Applications of magnetic resonance elastography to healthy and pathologic skeletal muscle. *J. Magn. Reson. Imaging* **2007**, *25*, 301–309. [CrossRef] [PubMed]

118. Debernard, L.; Robert, L.; Charleux, F.; Bensamoun, S.F. Analysis of thigh muscle stiffness from childhood to adulthood using magnetic resonance elastography (MRE) technique. *Clin. Biomech.* **2011**, *26*, 836–840. [CrossRef] [PubMed]

119. Palnitkar, H.; Reiter, R.O.; Majumdar, S.; Lewis, P.; Hammersley, M.; Shah, R.N.; Royston, T.J.; Klatt, D. An investigation into the relationship between inhomogeneity and wave shapes in phantoms and *ex vivo* skeletal muscle using magnetic resonance elastography and finite element analysis. *J. Mech. Behav. Biomed. Mater.* **2019**, *98*, 108–120. [CrossRef] [PubMed]

120. Qin, E.C.; Jugé, L.; Lambert, S.A.; Paradis, V.; Sinkus, R.; Bilston, L.E. *In vivo* anisotropic me-chanical properties of dystrophic skeletal muscles measured by anisotropic MR elastographic imaging: The mdx mouse model of muscular dystrophy. *Radiology* **2014**, *273*, 726–735. [CrossRef] [PubMed]

121. Green, M.A.; Geng, G.; Qin, E.; Sinkus, R.; Gandevia, S.C.; Bilston, L.E. Measuring anisotropic muscle stiffness properties using elastography. *NMR Biomed.* **2013**, *26*, 1387–1394. [CrossRef] [PubMed]

122. Smith, D.R.; Caban-Rivera, D.A.; Williams, L.T.; Van Houten, E.E.W.; Bayly, P.V.; Paulsen, K.D.; McGarry, M.D.J.; Johnson, C.L. *in vivo* estimation of anisotropic mechanical properties of the gastrocnemius during functional loading with MR elastography. *Phys. Med. Biol.* **2023**, *68*, 045004. [CrossRef] [PubMed]

123. Yin, M.; Venkatesh, S.K. Ultrasound or MR elastography of liver: Which one shall I use? *Abdom. Radiol.* **2018**, *43*, 1546–1551. [CrossRef] [PubMed]

124. Tahmasebi, A.; Wessner, C.E.; Guglielmo, F.F.; Wang, S.; Vu, T.; Liu, J.B.; Civan, J.; Lyshchik, A.; Forsberg, F.; Li, H.; et al. Comparison of magnetic resonance-based elas-tography and ultrasound shear wave elastography in patients with suspicion of nonal-coholic fatty liver disease. *Ultrasound Q.* **2023**, *39*, 100–108. [CrossRef] [PubMed]

125. Kennedy, P.; Bane, O.; Hectors, S.J.; Gordic, S.; Berger, M.; Delaney, V.; Salem, F.; Lewis, S.; Menon, M.; Taouli, B. Magnetic resonance elastography vs. point shear wave ultrasound elastography for the assessment of renal allograft dysfunction. *Eur. J. Radiol.* **2020**, *126*, 108949. [CrossRef] [PubMed]

126. Heers, G.; Jenkyn, T.; Dresner, M.A.; Klein, M.O.; Basford, J.R.; Kaufman, K.R.; Ehman, R.L.; An, K.N. Measurement of muscle activity with magnetic resonance elastography. *Clin. Biomech.* **2003**, *18*, 537–542. [CrossRef] [PubMed]

127. Schrank, F.; Warmuth, C.; Görner, S.; Meyer, T.; Tzschätzsch, H.; Guo, J.; Uca, Y.O.; Elgeti, T.; Braun, J.; Sack, I. Real-time MR elastography for viscoelasticity quantification in skeletal muscle during dynamic exercises. *Magn. Reson. Med.* **2020**, *84*, 103–114. [CrossRef] [PubMed]

128. Krivickas, L.S.; Dorer, D.J.; Ochala, J.; Frontera, W.R. Relationship between force and size in human single muscle fibres. *Exp. Physiol.* **2011**, *96*, 539–547. [CrossRef]

129. Jones, E.J.; Bishop, P.A.; Woods, A.K.; Green, J.M. Cross-sectional area and muscular strength. *Sports Med.* **2008**, *38*, 987–994. [CrossRef] [PubMed]

130. Reggiani, C.; Schiaffino, S. Muscle hypertrophy and muscle strength: Dependent or independent variables? A provocative review. *Eur. J. Transl. Myol.* **2020**, *30*, 9311. [CrossRef] [PubMed]

131. Ivey, F.M.; Tracy, B.L.; Lemmer, J.T.; NessAiver, M.; Metter, E.J.; Fozard, J.L.; Hurley, B.F. Effects of strength training and detraining on muscle quality: Age and gender comparisons. *J. Gerontol. A Biol. Sci. Med. Sci.* **2000**, *55*, B152–B159. [CrossRef] [PubMed]

132. Fukumoto, Y.; Ikezoe, T.; Yamada, Y.; Tsukagoshi, R.; Nakamura, M.; Mori, N.; Kimura, M.; Ichihashi, N. Skeletal muscle quality assessed from echo intensity is associated with muscle strength of middle-aged and elderly persons. *Eur. J. Appl. Physiol.* **2012**, *112*, 1519–1525. [CrossRef] [PubMed]

133. McGregor, R.A.; Cameron-Smith, D.; Poppitt, S.D. It is not just muscle mass: A review of muscle quality, composition and metabolism during ageing as determinants of muscle function and mobility in later life. *Longev. Health* **2014**, *3*, 9. [CrossRef] [PubMed]

134. Bogey, R.A.; Barnes, L.A. An EMG-to-Force Processing approach for estimating *in vivo* hip muscle forces in normal human walking. *IEEE Trans. Neural Syst. Rehabil. Eng.* **2017**, *25*, 1172–1179. [CrossRef] [PubMed]

135. Dieterich, A.V.; Botter, A.; Vieira, T.M.; Peolsson, A.; Petzke, F.; Davey, P.; Falla, D. Spatial variation and inconsistency between estimates of onset of muscle activation from EMG and ultrasound. *Sci. Rep.* **2017**, *7*, 42011. [CrossRef] [PubMed]

136. Maganaris, C.N.; Baltzopoulos, V.; Ball, D.; Sargeant, A.J. *In vivo* specific tension of human skeletal muscle. *J. Appl. Physiol.* **2001**, *90*, 865–872. [CrossRef] [PubMed]

137. Erskine, R.M.; Jones, D.A.; Maffulli, N.; Williams, A.G.; Stewart, C.E.; Degens, H. What causes *in vivo* muscle specific tension to increase following resistance training? *Exp. Physiol.* **2011**, *96*, 145–155. [CrossRef] [PubMed]

138. Chen, Z.; Franklin, D.W. Musculotendon parameters in lower limb models: Simplifications, uncertainties, and muscle force estimation sensitivity. *Ann. Biomed. Eng.* **2023**, *51*, 1147–1164. [CrossRef] [PubMed]

139. O'Brien, T.D.; Reeves, N.D.; Baltzopoulos, V.; Jones, D.A.; Maganaris, C.N. *In vivo* measurements of muscle specific tension in adults and children. *Exp. Physiol.* **2010**, *95*, 202–210. [CrossRef] [PubMed]

140. Brown, A.F. Ultrasonic spectroscopy in non-destructive testing. *Sci. Prog.* **1978**, *65*, 51–74.

141. Siegel, I.M.; Anast, G.T.; Fields, T. The determination of fracture healing by measurement of sound velocity across the fracture site. *Surg. Gynec Obs.* **1958**, *107*, 327–332.

142. Langton, C.M.; Palmer, S.B.; Porter, R.W. The measurement of broadband ultrasonic attenuation in cancellous bone. *Eng. Med.* **1984**, *13*, 89–91. [CrossRef] [PubMed]

143. Miles, C.A.; Fursey, G.A.; Birch, H.L.; Young, R.D. Factors affecting the ultrasonic properties of equine digital flexor tendons. *Ultrasound Med. Biol.* **1996**, *22*, 907–915. [CrossRef] [PubMed]

144. Langton, C.M.; Njeh, C.F. Sound-tissue interaction: The physical basis of bone ultrasonometry and limitations of existing methods. *J. Clin. Densitom.* **1998**, *1*, 295–301. [CrossRef] [PubMed]

145. Laugier, P. Instrumentation for *in vivo* ultrasonic characterization of bone strength. *IEEE Trans. Ultrason. Ferroelectr. Freq. Control* **2008**, *55*, 1179–1196. [CrossRef] [PubMed]

146. Njeh, C.F.; Fuerst, T.; Diessel, E.; Genant, H.K. Is quantitative ultrasound dependent on bone structure? A reflection. *Osteoporos. Int.* **2001**, *12*, 1–15. [CrossRef] [PubMed]

147. Muller, M.; Moilanen, P.; Bossy, E.; Nicholson, P.; Kilappa, V.; Timonen, J.; Talmant, M.; Cheng, S.; Laugier, P. Comparison of three ultrasonic axial transmission methods for bone assessment. *Ultrasound Med. Biol.* **2005**, *31*, 633–642. [CrossRef] [PubMed]

148. Pourcelot, P.; Defontaine, M.; Ravary, B.; Lemâtre, M.; Crevier-Denoix, N. A non-invasive method of tendon force measurement. *J. Biomech.* **2005**, *38*, 2124–2129. [CrossRef] [PubMed]

149. Vergari, C.; Ravary-Plumioën, B.; Evrard, D.; Laugier, P.; Mitton, D.; Pourcelot, P.; Crevier-Denoix, N. Axial speed of sound is related to tendon's nonlinear elasticity. *J. Biomech.* **2012**, *45*, 263–268. [CrossRef] [PubMed]

150. Dalle Carbonare, L.; Giannini, S. Bone microarchitecture as an important determinant of bone strength. *J. Endocrinol. Investig.* **2004**, *27*, 99–105. [CrossRef] [PubMed]

151. Laugier, P.; Droin, P.; Laval-Jeantet, A.M.; Berger, G. In vitro assessment of the relationship between acoustic properties and bone mass density of the calcaneus by comparison of ultrasound parametric imaging and quantitative computed tomography. *Bone* **1997**, *20*, 157–165. [CrossRef] [PubMed]

152. Langton, C.M. The 25th anniversary of BUA for the assessment of osteoporosis: Time for a new paradigm? *Proc. Inst. Mech. Eng. H J. Eng. Med.* **2011**, *225*, 113–125. [CrossRef] [PubMed]

153. Grimal, Q.; Laugier, P. Quantitative ultrasound assessment of cortical bone properties beyond bone mineral density. *IRBM* **2019**, *40*, 16–24. [CrossRef]

154. Minonzio, J.G.; Han, C.; Cassereau, D.; Grimal, Q. *In vivo* pulse-echo measurement of apparent broadband attenuation and Q factor in cortical bone: A preliminary study. *Phys. Med. Biol.* **2021**, *66*, 155002. [CrossRef] [PubMed]

155. Karjalainen, J.; Riekkinen, O.; Toyras, J.; Kroger, H.; Jurvelin, J. Ultrasonic assessment of cortical bone thickness in vitro and *in vivo*. *IEEE Trans. Ultrason. Ferroelectr. Freq. Control* **2008**, *55*, 2191–2197. [CrossRef] [PubMed]

156. Yamaguchi, T. Basic concept and clinical applications of quantitative ultrasound (QUS) technologies. *J. Med. Ultrason.* **2021**, *48*, 391–402. [CrossRef] [PubMed]

157. Hachiya, H.; Ohtsuki, S.; Tanaka, M.; Dunn, F. Determination of sound speed in biological tissues based on frequency analysis of pulse response. *J. Acoust. Soc. Am.* **1992**, *92*, 1564–1568. [CrossRef] [PubMed]

158. Sanabria, S.J.; Martini, K.; Freystätter, G.; Ruby, L.; Goksel, O.; Frauenfelder, T.; Rominger, M.B. Speed of sound ultrasound: A pilot study on a novel technique to identify sarcopenia in seniors. *Eur. J. Radiol.* **2019**, *29*, 3–12. [CrossRef] [PubMed]

159. Lowet, G.; Van der Perre, G. Ultrasound velocity measurement in long bones: Measurement method and simulation of ultrasound wave propagation. *J. Biomech.* **1996**, *29*, 1255–1262. [CrossRef]

160. Hans, D.; Srivastav, S.K.; Singal, C.; Barkmann, R.; Njeh, C.F.; Kantorovich, E.; Glüer, C.C.; Genant, H.K. Does combining the results from multiple bone sites measured by a new quantitative ultrasound device improve discrimination of hip fracture? *J. Bone Min. Res.* **1999**, *14*, 644–651. [CrossRef] [PubMed]

161. Camus, E.; Talmant, M.; Berger, G.; Laugier, P. Analysis of the axial transmission technique for the assessment of skeletal status. *J. Acoust. Soc. Am.* **2000**, *108*, 3058–3065. [CrossRef] [PubMed]

162. Bossy, E.; Talmant, M.; Laugier, P. Effect of bone cortical thickness on velocity measurements using ultrasonic axial transmission: A 2D simulation study. *J. Acoust. Soc. Am.* **2002**, *112*, 297–307. [CrossRef] [PubMed]

163. Saulgozis, J.; Pontaga, I.; Lowet, G.; Van der Perre, G. The effect of fracture and frac-ture fixation on ultrasonic velocity and attenuation. *Physiol. Meas.* **1996**, *17*, 201–211. [CrossRef] [PubMed]

164. Guglielmi, G.; de Terlizzi, F. Quantitative ultrasond in the assessment of osteoporosis. *Eur. J. Radiol.* **2009**, *71*, 425–431. [CrossRef] [PubMed]

165. Njeh, C.F.; Hodgkinson, R.; Currey, J.D.; Langton, C.M. Orthogonal relationships between ultrasonic velocity and material properties of bovine cancellous bone. *Med. Eng. Phys.* **1996**, *18*, 373–381. [CrossRef] [PubMed]

166. Nicholson, P.H.; Strelitzki, R. On the prediction of Young's modulus in calcaneal cancellous bone by ultrasonic bulk and bar velocity measurements. *Clin. Rheumatol.* **1999**, *18*, 10–16. [CrossRef]

167. Vergari, C.; Pourcelot, P.; Holden, L.; Ravary-Plumioen, B.; Gerard, G.; Laugier, P.; Mitton, D.; Crevier-Denoix, N. True stress and Poisson's ratio of tendons during loading. *J. Biomech.* **2011**, *44*, 719–724. [CrossRef] [PubMed]

168. Kuo, P.L.; Li, P.C.; Li, M.L. Elastic properties of tendon measured by two different approaches. *Ultrasound Med. Biol.* **2001**, *27*, 1275–1284. [CrossRef] [PubMed]

169. Crevier-Denoix, N.; Ravary-Plumioen, B.; Evrard, D.; Pourcelot, P. Reproducibility of a non-invasive ultrasonic technique of tendon force measurement, determined in vitro in equine superficial digital flexor tendons. *J. Biomech.* **2009**, *42*, 2210–2213. [CrossRef]

170. Korta Martiartu, N.; Nakhostin, D.; Ruby, L.; Frauenfelder, T.; Rominger, M.B.; Sanabria, S.J. Speed of sound and shear wave speed for calf soft tissue composition and nonlinearity assessment. *Quant. Imaging Med. Surg.* **2021**, *11*, 4149–4161. [CrossRef] [PubMed]

171. Ooi, C.C.; Malliaras, P.; Schneider, M.E.; Connell, D.A. "Soft, hard, or just right?" Applications and limitations of axial-strain sonoelastography and shear-wave elastography in the assessment of tendon injuries. *Skelet. Radiol.* **2014**, *43*, 1–12. [CrossRef] [PubMed]

172. Pourcelot, P.; van den Bogert, A.J.; Huang, X.; Crevier-Denoix, N. Achilles tendon loads at walk measured using a novel ultrasonic technique. *Comput. Methods Biomech. Biomed. Eng.* **2005**, *8*, 221–222. [CrossRef]

173. Brauner, T.; Hooper, S.L.; Pourcelot, P.; Crevier-Denoix, N.; Horstmann, T.; Wearing, S.C. Load in the Achilles tendon is progressively increased with reductions in walking speed. *Med. Sci. Sports Exerc.* **2017**, *49*, 2001–2008. [CrossRef] [PubMed]

174. Wearing, S.C.; Kuhn, L.; Pohl, T.; Horstmann, T.; Brauner, T. Transmission-mode ultrasound for monitoring the instantaneous elastic modulus of the achilles tendon during unilateral submaximal vertical hopping. *Front. Physiol.* **2020**, *11*, 567641. [CrossRef] [PubMed]

175. Smith, N.B.; Webb, A.G. *Introduction to Medical Imaging: Physics, Engineering and Clinical Applications*; Cambridge University Press: Cambridge, UK, 2001.

176. Wu, K.; Xue, Q.; Adler, L. Reflection and transmission of elastic waves from a fluid saturated porous solid boundary. *J. Acoust. Soc. Am.* **1990**, *87*, 2349–2358. [CrossRef]

177. Verhoef, W.A.; Cloostermans, M.J.T.M.; Thijssen, J.M. Diffraction and dispersion effects on the estimation of ultrasound attenuation and velocity in biological tissues. *IEEE Trans. Biomed. Eng.* **1985**, *32*, 521–529. [CrossRef] [PubMed]

178. Petley, G.W.; Robins, P.A.; Aindow, J.D. Broadband ultrasonic attenuation: Are current measurement techniques inherently inaccurate? *Br. J. Radiol.* **1995**, *68*, 1212–1214. [CrossRef] [PubMed]

179. Wear, K.A. Mechanisms of interaction of ultrasound with cancellous bone: A review. *IEEE Trans. Ultrason. Ferroelectr. Freq. Control* **2020**, *67*, 454–482. [CrossRef] [PubMed]

180. Chaffai, S.; Padilla, F.; Berger, G.; Laugier, P. In vitro measurement of the frequency-dependent attenuation in cancellous bone between 0.2 and 2 MHz. *J. Acoust. Soc. Am.* **2000**, *108*, 1281–1289. [CrossRef] [PubMed]

181. Wear, K.A. Ultrasonic attenuation in human calcaneus from 0.2 to 1.7 MHz. *IEEE Trans. Ultrason. Ferroelectr. Freq. Control* **2001**, *48*, 602–608. [CrossRef] [PubMed]

182. Quarato, C.M.I.; Lacedonia, D.; Salvemini, M.; Tuccari, G.; Mastrodonato, G.; Villani, R.; Fiore, L.A.; Scioscia, G.; Mirijello, A.; Saponara, A.; et al. A review on biological effects of ultrasounds: Key messages for clinicians. *Diagnostics* **2023**, *13*, 855. [CrossRef] [PubMed]

183. Azhari, H. *Basics of Biomedical Ultrasound for Engineers*; John Wiley & Sons, Inc.: Hoboken, NJ, USA, 2010; p. 392.

184. Dussik, K.T.; Fritch, D.J.; Kyriazidou, M.; Sear, R.S. Measurements of articular tissues with ultrasound. *Am. J. Phys. Med.* **1958**, *37*, 160–165. [CrossRef] [PubMed]

185. Rho, J.Y.; Ashman, R.B.; Turner, C.H. Young's modulus of trabecular and cortical bone material: Ultrasonic and microtensile measurements. *J. Biomech.* **1993**, *26*, 111–119. [CrossRef] [PubMed]

186. Natali, A.N.; Meroi, E.A. A review of the biomechanical properties of bone as a material. *J. Biomed. Eng.* **1989**, *11*, 266–276. [CrossRef] [PubMed]

187. Hasgall, P.A.; Di Gennaro, F.; Baumgartner, C.; Neufeld, E.; Lloyd, B.; Gosselin, M.C.; Payne, D.; Klingenböck, A.; Kuster, N. *IT'IS Database for Thermal and Electromagnetic Parameters of Biological Tissues*, Version 4.1; 2022. Available online: https://itis.swiss/virtual-population/tissue-properties/downloads/database-v4-1/ (accessed on 19 June 2024). [CrossRef]

188. Abendschein, W.; Hyatt, G.W. Ultrasonics and selected physical properties of bone. *Clin. Orthop. Relat. Res.* **1970**, *69*, 294–301. [CrossRef] [PubMed]

189. Han, S.; Rho, J.; Medige, J.; Ziv, I. Ultrasound velocity and broadband attenuation over a wide range of bone mineral density. *Osteoporos. Int.* **1996**, *6*, 291–296. [CrossRef] [PubMed]

190. Fuerst, T.; Genant, H.K.; Gluer, C.C.; Hans, D.; Njeh, C.F. *Quantitative Ultrasound: Assessment of Osteoporosis and Bone Status*; Taylor & Francis: Abingdon, UK, 1999.

191. Ashman, R.B.; Rho, J.Y. Elastic modulus of trabecular bone material. *J. Biomech.* **1988**, *21*, 177–181. [CrossRef] [PubMed]

192. Keaveny, T.M.; Hayes, W.C. A 20-year perspective on the mechanical properties of trabecular bone. *J. Biomech. Eng.* **1993**, *115*, 534–542. [CrossRef] [PubMed]

193. Garcia, T.; Hornof, W.J.; Insana, M.F. On the ultrasonic properties of tendon. *Ultrasound Med. Biol.* **2003**, *29*, 1787–1797. [CrossRef]

194. Bennett, M.B.; Ker, R.F.; Imery, N.J.; Alexander, R.M. Mechanical properties of various mammalian tendons. *J. Zool.* **1986**, *209*, 537–548. [CrossRef]

195. Mast, T.D.; Hinkelman, L.M.; Orr, M.J.; Sparrow, V.W.; Waag, R.C. Simulation of ultrasonic pulse propagation through the abdominal wall. *J. Acoust. Soc. Am.* **1997**, *102*, 1177–1190. [CrossRef]

196. Mast, T.D. Empirical relationships between acoustic parameters in human soft tissues. *Acoust. Res. Lett. Online* **2000**, *1*, 37. [CrossRef]

197. Culjat, M.O.; Goldenberg, D.; Tewari, P.; Singh, R.S. A review of tissue substitutes for ultrasound imaging. *J. Ultrasound Med. Biol.* **2010**, *36*, 861–873. [CrossRef]

198. Keshavarzi, A.; Vaezy, S.; Kaczkowski, P.J.; Keilman, G.; Martin, R.; Chi, E.Y.; Garcia, R.; Fujimoto, V.Y. Attenuation coefficient and sound speed in human myometrium and uterine fibroid tumors. *J. Ultrasound Med.* **2001**, *20*, 473–480. [CrossRef]

199. Nassiri, D.K.; Nicholas, D.; Hill, C.R. Attenuation of ultrasound in skeletal muscle. *Ultrasonics* **1979**, *17*, 230–232. [CrossRef] [PubMed]

200. Fernandez, S.V.; Kim, J.-H.; Sadat, D.; Marcus, C.; Suh, E.; Mclntosh, R.; Shah, A.; Dagdeviren, C. A dynamic ultrasound phantom with tissue-mimicking mechanical and acoustic properties. *Adv. Sci.* **2024**, *11*, 2400271. [CrossRef]

201. Shepherd, J.A. Positions of the international society for clinical densitometry and their etiology: A scoping review. *J. Clin. Densitom.* **2023**, *26*, 101369. [CrossRef]

202. Lancaster, E.K.; Evans, R.A.; Kos, S.; Hills, E.; Dunstan, C.R.; Wong, S.Y. Measurement of bone in the os calcis: A clinical evaluation. *J. Bone Min. Res.* **1989**, *4*, 507–514. [CrossRef]

203. Sone, T.; Imai, Y.; Tomomitsu, T.; Fukunaga, M. Calcaneus as a site for the assessment of bone mass. *Bone* **1998**, *22*, 155S–157S. [CrossRef]

204. Barkmann, R.; Laugier, P.; Moser, U.; Dencks, S.; Klausner, M.; Padilla, F.; Haiat, G.; Hel-ler, M.; Gluer, C.C. *In vivo* measurements of ultrasound transmission through the human proximal femur. *Ultrasound Med. Biol.* **2008**, *34*, 1186–1190. [CrossRef]

205. Gnudi, S.; Malavolta, N.; Calderoni, P.; Bettelli, G.; Gualtieri, G. Ultrasound in the evaluation of bone fragility caused by osteoporosis: A comparison between different sites of measurement. *Chir. Organi Mov.* **1996**, *81*, 383–387.

206. Gnudi, S.; Ripamonti, C.; Malavolta, N. Quantitative ultrasound and bone densitometry to evaluate the risk of nonspine fractures: A prospective study. *Osteoporos. Int.* **2000**, *11*, 518–523. [CrossRef] [PubMed]

207. Barkmann, R.; Rohrschneider, W.; Vierling, M.; Tröger, J.; de Terlizzi, F.; Cadossi, R.; Heller, M.; Glüer, C.C. German pediatric reference data for quantitative transverse transmission ultrasound of finger phalanges. *Osteoporos. Int.* **2002**, *13*, 55–61. [CrossRef] [PubMed]

208. Gerlanc, M.; Haddad, D.; Hyatt, G.W.; Langloh, J.T.; St Hilaire, P. Ultrasonic study of normal and fractured bone. *Clin. Orthop. Relat. Res.* **1975**, *111*, 175–180. [CrossRef] [PubMed]

209. Raum, K.; Laugier, P. Clinical devices for bone assessment. *Adv. Exp. Med. Biol.* **2022**, *1364*, 35–53. [CrossRef] [PubMed]

210. Mathieu, V.; Chappard, C.; Vayron, R.; Michel, A.; Haïat, G. Radial anatomic variation of ultrasonic velocity in human cortical bone. *Ultrasound Med. Biol.* **2013**, *39*, 2185–2193. [CrossRef] [PubMed]

211. Langton, C.M.; Langton, D.K. Male and female normative data for ultrasound measurement of the calcaneus within the UK adult population. *Br. J. Radiol.* **1997**, *70*, 580–585. [CrossRef] [PubMed]

212. Heldan de Moura Castro, C.; Medeiros Pinheiro, M.; Lúcia Szejnfeld, V. Quantitative ultrasound of the calcaneus in Brazilian Caucasian women: Normative data are similar to the manufacturer's normal range. *Osteoporos. Int.* **2000**, *11*, 923–928. [CrossRef] [PubMed]

213. Kastelan, D.; Kujundzic-Tiljak, M.; Kraljevic, I.; Kardum, I.; Giljevic, Z.; Korsic, M. Calcaneus ultrasound in males: Normative data in the Croatian population (ECUM study). *J. Endocrinol. Investig.* **2006**, *29*, 221–225. [CrossRef] [PubMed]

214. Drake, W.M.; McClung, M.; Njeh, C.F.; Genant, H.K.; Rosen, C.; Watts, N.; Kendler, D.L. Multisite bone ultrasound measurement on North American female reference population. *J. Clin. Densitom.* **2001**, *4*, 239–248. [CrossRef] [PubMed]

215. Hayman, S.R.; Drake, W.M.; Kendler, D.L.; Olszynski, W.P.; Webber, C.E.; Rosen, C.J.; Genant, H.K.; Orwoll, E.S.; Pickard, L.E.; Adachi, J.D. North American male reference population for speed of sound in bone at multiple skeletal sites. *J. Clin. Densitom.* **2002**, *5*, 63–71. [CrossRef] [PubMed]

216. Hans, D.; Wu, C.; Njeh, C.; Zhao, S.; Augat, P.; Newitt, D.; Link, T.; Lu, Y.; Majumdar, S.; Genant, H.K. Ultrasound velocity of trabecular cubes reflects mainly bone density and elasticity. *Calcif. Tissue Int.* **1999**, *64*, 18–23. [CrossRef] [PubMed]

217. Bouxsein, M.L.; Radloff, S.E. Quantitative ultrasound of the calcaneus reflects the mechanical properties of calcaneal trabecular bone. *J. Bone Min. Res.* **1997**, *12*, 839–846. [CrossRef] [PubMed]

218. Toyras, J.; Kroger, H.; Jurvelin, J.S. Bone properties as estimated by mineral density, ultrasound attenuation, and velocity. *Bone* **1999**, *25*, 725–731. [CrossRef] [PubMed]

219. Toyras, J.; Nieminen, M.T.; Kroger, H.; Jurvelin, J.S. Bone mineral density, ultrasound velocity, and broadband attenuation predict mechanical properties of trabecular bone differently. *Bone* **2002**, *31*, 503–507. [CrossRef] [PubMed]

220. Cortet, B.; Boutry, N.; Dubois, P.; Legroux-Gérot, I.; Cotten, A.; Marchandise, X. Does quantitative ultrasound of bone reflect more bone mineral density than bone microarchitecture? *Calcif. Tissue Int.* **2004**, *74*, 60–67. [CrossRef] [PubMed]

221. Trebacz, H.; Natali, A. Ultrasound velocity and attenuation in cancellous bone samples from lumbar vertebra and calcaneus. *Osteoporos. Int.* **1999**, *9*, 99–105. [CrossRef] [PubMed]

222. Padilla, F.; Jenson, F.; Bousson, V.; Peyrin, F.; Laugier, P. Relationships of trabecular bone structure with quantitative ultrasound parameters: In vitro study on human proximal fe-mur using transmission and backscatter measurements. *Bone* **2008**, *42*, 1193–1202. [CrossRef] [PubMed]

223. McCloskey, E.V.; Murray, S.A.; Charlesworth, D.; Miller, C.; Fordham, J.; Clifford, K.; Atkins, R.; Kanis, J.A. Assessment of broadband ultrasound attenuation in the os calcis in vitro. *Clin. Sci.* **1990**, *78*, 221–225. [CrossRef]

224. Hollaender, R.; Hartl, F.; Krieg, M.A.; Tyndall, A.; Geuckel, C.; Buitrago-Tellez, C.; Manghani, M.; Kraenzlin, M.; Theiler, R.; Hans, D. Prospective evaluation of risk of vertebral fractures using quantitative ultrasound measurements and bone mineral density in a population-based sample of postmenopausal women: Results of the Basel Osteoporosis Study. *Ann. Rheum. Dis.* **2009**, *68*, 391–396. [CrossRef] [PubMed]

225. McCloskey, E.V.; Kanis, J.A.; Odén, A.; Harvey, N.C.; Bauer, D.; González-Macias, J.; Hans, D.; Kaptoge, S.; Krieg, M.A.; Kwok, T.; et al. Predictive ability of heel quantitative ul-trasound for incident fractures: An individual-level meta-analysis. *Osteoporos. Int.* **2015**, *26*, 1979–1987. [CrossRef] [PubMed]

226. Marin, F.; Gonzalez-Macias, J.; Diez-Perez, A.; Palma, S.; Delgado-Rodriguez, M. Relationship between bone quantitative ultrasound and fractures: A meta-analysis. *J. Bone Min. Res.* **2006**, *21*, 1126–1135. [CrossRef] [PubMed]

227. Moayyeri, A.; Adams, J.E.; Adler, R.A.; Krieg, M.A.; Hans, D.; Compston, J.; Lewiecki, E.M. Quantitative ultrasound of the heel and fracture risk assessment: An updated meta-analysis. *Osteoporos. Int.* **2012**, *23*, 143–153. [CrossRef] [PubMed]

228. Glüer, C.C.; Eastell, R.; Reid, D.M.; Felsenberg, D.; Roux, C.; Barkmann, R.; Timm, W.; Blenk, T.; Armbrecht, G.; Stewart, A.; et al. Association of five quantitative ultrasound devices and bone densitometry with osteoporotic vertebral fractures in a population-based sample: The OPUS Study. *J. Bone Min. Res.* **2004**, *19*, 782–793. [CrossRef] [PubMed]

229. Hans, D.; Baim, S. Quantitative ultrasound (QUS) in the management of osteoporosis and assessment of fracture risk. *J. Clin. Densitom.* **2017**, *20*, 322–333. [CrossRef] [PubMed]

230. Huang, C.; Ross, P.D.; Yates, A.J.; Walker, R.E.; Imose, K.; Emi, K.; Wasnich, R.D. Prediction of fracture risk by radiographic absorptiometry and quantitative ultrasound: A prospective study. *Calcif. Tissue Int.* **1998**, *63*, 380–384. [CrossRef] [PubMed]

231. Lasschuit, J.W.J.; Center, J.R.; Greenfield, J.R.; Tonks, K.T.T. Comparison of calcaneal quantitative ultrasound and bone den-sitometry parameters as fracture risk predictors in type 2 diabe-tes mellitus. *Diabet. Med.* **2020**, *37*, 1902–1909. [CrossRef] [PubMed]

232. McCloskey, E.V.; Murray, S.A.; Miller, C.; Charlesworth, D.; Tindale, W.; O'Doherty, D.P.; Bickerstaff, D.R.; Hamdy, N.A.; Kanis, J.A. Broadband ultrasound attenuation in the os calcis: Relationship to bone mineral at other skeletal sites. *Clin. Sci.* **1990**, *78*, 227–233. [CrossRef] [PubMed]

233. Anna, U.M.; Maria, S.; Kerstin, B. Comparison of quantitative ultrasound of calcaneus and dual energy X-ray absorptiometry in measuring bone density and predicting fractures in patients with diabetic polyneuropathy: A prospective cohort study. *Diabetes Res. Clin. Pr.* **2021**, *180*, 109064. [CrossRef] [PubMed]

234. Vestergaard, P. Discrepancies in bone mineral density and fracture risk in patients with type 1 and type 2 diabetes—A meta-analysis. *Osteoporos. Int.* **2007**, *18*, 427–444. [CrossRef] [PubMed]

235. Raisi-Estabragh, Z.; Biasiolli, L.; Cooper, J.; Aung, N.; Fung, K.; Paiva, J.M.; Sanghvi, M.M.; Thomson, R.J.; Curtis, E.; Paccou, J.; et al. Poor bone quality is associated with greater arterial stiffness: Insights from the UK Biobank. *J. Bone Min. Res.* **2021**, *36*, 90–99. [CrossRef]

236. Gebre, A.K.; Prince, R.L.; Schousboe, J.T.; Kiel, D.P.; Thompson, P.L.; Zhu, K.; Lim, W.H.; Sim, M.; Lewis, J.R. Calcaneal quantitative ultrasound is associated with all-cause and cardiovascular disease mortality independent of hip bone mineral density. *Osteoporos. Int.* **2022**, *33*, 1557–1567. [CrossRef]

237. Foldes, A.J.; Rimon, A.; Keinan, D.; Popovtzer, M. Quantitative ultrasound of the tibia: A novel approach for assessment of bone status. *Bone* **1995**, *17*, 363–367. [CrossRef]

238. Nishiyama, K.K.; Macdonald, H.M.; Buie, H.R.; Hanley, D.A.; Boyd, S.K. Postmenopausal women with osteopenia have higher cortical porosity and thinner cortices at the distal radius and tibia than women with normal aBMD: An *in vivo* HR-pQCT study. *J. Bone Min. Res.* **2010**, *25*, 882–890. [CrossRef]

239. Shigdel, R.; Osima, M.; Ahmed, L.A.; Joakimsen, R.M.; Eriksen, E.F.; Zebaze, R.; Bjørnerem, Å. Bone turnover markers are associated with higher cortical porosity, thinner cortices, and larger size of the proximal femur and non-vertebral fractures. *Bone* **2015**, *81*, 1–6. [CrossRef]

240. Bossy, E.; Talmant, M.; Peyrin, F.; Akrout, L.; Cloetens, P.; Laugier, P. An in vitro study of the ultrasonic axial transmission technique at the radius: 1-MHz velocity measurements are sensitive to both mineralization and intracortical porosity. *J. Bone Min. Res.* **2004**, *19*, 1548–1556. [CrossRef]

241. Nicholson, P.H.; Moilanen, P.; Kärkkäinen, T.; Timonen, J.; Cheng, S. Guided ultrasonic waves in long bones: Modelling, experiment and *in vivo* application. *Physiol. Meas.* **2002**, *23*, 755–768. [CrossRef]

242. Weiss, M.; Ben-Shlomo, A.B.; Hagag, P.; Rapoport, M. Reference database for bone speed of sound measurement by a novel quantitative multi-site ultrasound device. *Osteoporos. Int.* **2000**, *11*, 688–696. [CrossRef]

243. Barkmann, R.; Kantorovich, E.; Singal, C.; Hans, D.; Genant, H.K.; Heller, M.; Glüer, C.C. A new method for quantitative ultrasound measurements at multiple skeletal sites: First results of precision and fracture discrimination. *J. Clin. Densitom.* **2000**, *3*, 1–7. [CrossRef]

244. Weiss, M.; Ben-Shlomo, A.; Hagag, P.; Ish-Shalom, S. Discrimination of proximal hip fracture by quantitative ultrasound measurement at the radius. *Osteoporos. Int.* **2000**, *11*, 411–416. [CrossRef]

245. Njeh, C.F.; Saeed, I.; Grigorian, M.; Kendler, D.L.; Fan, B.; Shepherd, J.; McClung, M.; Drake, W.M.; Genant, H.K. Assessment of bone status using speed of sound at multiple anatomical sites. *Ultrasound Med. Biol.* **2001**, *27*, 1337–1345. [CrossRef] [PubMed]

246. Clowes, J.A.; Eastell, R.; Peel, N.F. The discriminative ability of peripheral and axial bone measurements to identify proximal femoral, vertebral, distal forearm and proximal humeral fractures: A case control study. *Osteoporos. Int.* **2005**, *16*, 1794–1802. [CrossRef] [PubMed]

247. Damilakis, J.; Papadokostakis, G.; Perisinakis, K.; Maris, T.; Dimitriou, P.; Hadjipavlou, A.; Gourtsoyiannis, N. Discrimination of hip fractures by quantitative ultrasound of the phalanges and the calcaneus and dual X-ray absorptiometry. *Eur. J. Radiol.* **2004**, *50*, 268–272. [CrossRef] [PubMed]

248. Dobnig, H.; Piswanger-Sölkner, J.C.; Obermayer-Pietsch, B.; Tiran, A.; Strele, A.; Maier, E.; Maritschnegg, P.; Riedmüller, G.; Brueck, C.; Fahrleitner-Pammer, A. Hip and nonvertebral fracture prediction in nursing home patients: Role of bone ultrasound and bone marker measurements. *J. Clin. Endocrinol. Metab.* **2007**, *92*, 1678–1686. [CrossRef] [PubMed]

249. Lee, S.H.; Khang, Y.H.; Lim, K.H.; Kim, B.J.; Koh, J.M.; Kim, G.S.; Kim, H.; Cho, N.H. Clinical risk factors for osteoporotic fracture: A population-based prospective cohort study in Korea. *J. Bone Min. Res.* **2010**, *25*, 369–378. [CrossRef] [PubMed]

250. Olszynski, W.P.; Brown, J.P.; Adachi, J.D.; Hanley, D.A.; Ioannidis, G.; Davison, K.S.; CaMos Research Group. Multisite quantitative ultrasound for the prediction of fractures over 5 years of follow-up: The Canadian Multicentre Osteoporosis Study. *J. Bone Min. Res.* **2013**, *28*, 2027–2034. [CrossRef] [PubMed]

251. Olszynski, W.P.; Davison, K.S.; Adachi, J.D.; Brown, J.P.; Hanley, D.A. Change in quantitative ultrasound-assessed speed of sound as a function of age in women and men and association with the use of antiresorptive agents: The Canadian Multicentre Osteoporosis Study. *J. Clin. Densitom.* **2020**, *23*, 549–560. [CrossRef] [PubMed]

252. Wang, Q.; Nicholson, P.H.; Timonen, J.; Alen, M.; Moilanen, P.; Suominen, H.; Cheng, S. Monitoring bone growth using quantitative ultrasound in comparison with DXA and pQCT. *J. Clin. Densitom.* **2008**, *11*, 295–301. [CrossRef] [PubMed]

253. Lee, S.C.; Coan, B.S.; Bouxsein, M.L. Tibial ultrasound velocity measured in situ predicts the material properties of tibial cortical bone. *Bone* **1997**, *21*, 119–125. [CrossRef] [PubMed]

254. Stegman, M.R.; Heaney, R.P.; Travers, G.D.; Leist, J. Cortical ultrasound velocity as an indicator of bone status. *Osteoporos. Int.* **1995**, *5*, 349–353. [CrossRef]

255. Dodd, S.P.; Cunningham, J.L.; Miles, A.W.; Gheduzzi, S.; Humphrey, V.F. Ultrasound transmission loss across transverse and oblique bone fractures: An in vitro study. *Ultrasound Med. Biol.* **2008**, *34*, 454–462. [CrossRef] [PubMed]

256. Machado, C.B.; de Albuquerque Pereira, W.C.; Talmant, M.; Padilla, F.; Laugier, P. Computational evaluation of the compositional factors in fracture healing affecting ultrasound axial transmission measurements. *Ultrasound Med. Biol.* **2010**, *36*, 1314–1326. [CrossRef] [PubMed]

257. Machado, C.B.; Pereira, W.C.; Granke, M.; Talmant, M.; Padilla, F.; Laugier, P. Experimental and simulation results on the effect of cortical bone mineralization in ultrasound axial transmission measurements: A model for fracture healing ultrasound monitoring. *Bone* **2011**, *48*, 1202–1209. [CrossRef] [PubMed]

258. Potsika, V.T.; Spiridon, I.F.; Protopappas, V.C.; Vavva, M.G.; Lymperopoulos, P.D.; Massalas, C.V.; Polyzos, D.K.; Fotiadis, D.I. Computational study of the influence of callus porosity on ultra-sound propagation in healing bones. *Annu. Int. Conf. IEEE Eng. Med. Biol. Soc.* **2014**, *2014*, 684–687. [CrossRef] [PubMed]

259. Gheduzzi, S.; Dodd, S.P.; Miles, A.W.; Humphrey, V.F.; Cunningham, J.L. Numerical and experimental simulation of the effect of long bone fracture healing stages on ultrasound transmission across an idealized fracture. *J. Acoust. Soc. Am.* **2009**, *126*, 887–894. [CrossRef] [PubMed]

260. Protopappas, V.C.; Vavva, M.G.; Fotiadis, D.I.; Malizos, K.N. Ultrasonic monitoring of bone fracture healing. *IEEE Trans. Ultrason. Ferroelectr. Freq. Control* **2008**, *55*, 1243–1255. [CrossRef] [PubMed]

261. Potsika, V.T.; Grivas, K.N.; Protopappas, V.C.; Vavva, M.G.; Raum, K.; Rohrbach, D.; Polyzos, D.; Fotiadis, D.I. Application of an effective medium theory for modeling ultrasound wave propagation in healing long bones. *Ultrasonics* **2014**, *54*, 1219–1230. [CrossRef] [PubMed]

262. Xu, K.; Ta, D.; He, R.; Qin, Y.-X.; Wang, W. Axial transmission method for long bone fracture evaluation by ultrasonic guided waves: Simulation, phantom and in vitro experiments. *Ultrasound Med. Biol.* **2014**, *40*, 817–827. [CrossRef] [PubMed]

263. Li, Y.; Liu, D.; Xu, K.; Ta, D.; Le, L.H.; Wang, W. Transverse and oblique long bone fracture evaluation by low order ultrasonic guided waves: A simulation study. *Biomed. Res. Int.* **2017**, *2017*, 3083141. [CrossRef] [PubMed]

264. Xie, Y.; Chen, S.; Wan, X.; Tse, P.W. A preliminary numerical study on the interactions between nonlinear ultrasonic guided waves and a single crack in bone materials with motivation to the evaluation of micro cracks in long bones. *IEEE Access* **2020**, *8*, 169169–169182. [CrossRef]

265. Lefebvre, F.; Deblock, Y.; Campistron, P.; Ahite, D.; Fabre, J.J. Development of a new ultrasonic technique for bone and biomaterials in vitro characterization. *J. Biomed. Mater. Res.* **2002**, *63*, 441–446. [CrossRef] [PubMed]

266. Moilanen, P.; Talmant, M.; Nicholson, P.H.F.; Cheng, S.; Timonen, J.; Laugier, P. Ultrasonically determined thickness of long cortical bones: Three-dimensional simulations of in vitro experiments. *J. Acoust. Soc. Am.* **2007**, *122*, 2439–2445. [CrossRef] [PubMed]

267. Foiret, J.; Minonzio, J.-G.; Chappard, C.; Talmant, M.; Laugier, P. Combined estimation of thickness and velocities using ultrasound guided waves: A pioneering study on in vitro cortical bone samples. *IEEE Trans. Ultrason. Ferroelectr. Freq. Control* **2014**, *61*, 1478–1488. [CrossRef] [PubMed]

268. Vallet, Q.; Bochud, N.; Chappard, C.; Laugier, P.; Minonzio, J.G. *In vivo* characterization of cortical bone using guided waves measured by axial transmission. *IEEE Trans. Ultrason. Ferroelectr. Freq. Control* **2016**, *63*, 1361–1371. [CrossRef] [PubMed]

269. Minonzio, J.; Bochud, N.; Vallet, Q.; Ramiandrisoa, D.; Etcheto, A.; Briot, K.; Kolta, S.; Roux, C.; Laugier, P. Ultrasound-based estimates of cortical bone thickness and porosity are associated with nontraumatic fractures in postmenopausal women: A pilot study. *J. Bone Min. Res.* **2019**, *34*, 1585–1596. [CrossRef] [PubMed]

270. Minonzio, J.G.; Ramiandrisoa, D.; Schneider, J.; Kohut, E.; Streichhahn, M.; Stervbo, U.; Wirth, R.; Westhoff, T.H.; Raum, K.; Babel, N. Bi-Directional Axial Transmission measurements applied in a clinical environment. *PLoS ONE* **2022**, *17*, e0277831. [CrossRef] [PubMed]

271. Yang, Z.; Yang, H.; Tian, T.; Deng, D.; Hu, M.; Ma, J.; Gao, D.; Zhang, J.; Ma, S.; Yang, L.; et al. A review on guided-ultrasonic-wave-based structural health monitoring: From fundamental theory to machine learning techniques. *Ultrasonics* **2023**, *133*, 107014. [CrossRef] [PubMed]

272. Moilanen, P. Ultrasonic guided waves in bone. *IEEE Trans. Ultrason. Ferroelectr. Freq. Control* **2008**, *55*, 1277–1286. [CrossRef]

273. Craven, J.D.; Costantini, M.A.; Greenfield, M.A.; Stern, R. Measurement of the velocity of ultrasound in human cortical bone and its potential clinical importance. An *in vivo* preliminary study. *Investig. Radiol.* **1973**, *8*, 72–77. [CrossRef] [PubMed]

274. Greenfield, M.A.; Craven, J.D.; Huddleston, A.; Kehrer, M.L.; Wishko, D.; Stern, R. Measurement of the velocity of ultrasound in human cortical bone *in vivo*. Estimation of its potential value in the diagnosis of osteoporosis and metabolic bone disease. *Radiology* **1981**, *138*, 701–710. [CrossRef] [PubMed]

275. Hyödynmaa, S.J.; Karellas, A.; Whiting, J.S.; Craven, J.D.; Greenfield, M.A. *In vivo* measurement of the ultrasound attenuation coefficient in cortical bone. *Med. Phys.* **1981**, *8*, 555.

276. Currey, J.D. The effect of porosity and mineral content on the Young's modulus of elasticity of compact bone. *J. Biomech.* **1988**, *21*, 131–139. [CrossRef] [PubMed]

277. Schaffler, M.B.; Burr, D.B. Stiffness of compact bone: Effects of porosity and density. *J. Biomech.* **1988**, *21*, 13–16. [CrossRef] [PubMed]

278. Wear, K.A. Autocorrelation and cepstral methods for measurement of tibial cortical thickness. *IEEE Trans. Ultrason. Ferroelectr. Freq. Control* **2003**, *50*, 655–660. [CrossRef] [PubMed]

279. Schousboe, J.T.; Riekkinen, O.; Karjalainen, J. Prediction of hip osteoporosis by DXA using a novel pulse-echo ultrasound device. *Osteoporos. Int.* **2017**, *28*, 85–93. [CrossRef] [PubMed]

280. Karjalainen, J.P.; Riekkinen, O.; Kröger, H. Pulse-echo ultrasound method for detection of post-menopausal women with osteoporotic BMD. *Osteoporos. Int.* **2018**, *29*, 1193–1199. [CrossRef] [PubMed]

281. Karjalainen, J.P.; Riekkinen, O.; Töyräs, J.; Hakulinen, M.; Kröger, H.; Rikkonen, T.; Salovaara, K.; Jurvelin, J.S. Multi-site bone ultrasound measurements in elderly women with and without previous hip fractures. *Osteoporos. Int.* **2012**, *23*, 1287–1295. [CrossRef] [PubMed]

282. Lewiecki, E.M. Pulse-echo ultrasound identifies caucasian and hispanic women at risk for osteoporosis. *J. Clin. Densitom.* **2020**, *24*, 175–182. [CrossRef] [PubMed]

283. Dovjak, P.; Iglseder, B.; Rainer, A.; Dovjak, G.; Weber, M.; Pietschmann, P. Pulse-echo ultra-sound measurement in osteoporosis screening: A pilot study in older patients. *Aging Clin. Exp. Res.* **2023**, *35*, 1221–1230. [CrossRef] [PubMed]

284. Wear, K.A.; Armstrong, D.W., 3rd. Relationships among calcaneal backscatter, attenuation, sound speed, hip bone mineral density, and age in normal adult women. *J. Acoust. Soc. Am.* **2001**, *110*, 573–578. [CrossRef] [PubMed]

285. Iori, G.; Du, J.; Hackenbeck, J.; Kilappa, V.; Raum, K. Estimation of cortical bone microstructure from ultrasound backscatter. *IEEE Trans. Ultrason. Ferroelectr. Freq. Control* **2021**, *68*, 1081–1095. [CrossRef] [PubMed]

286. Litniewski, J.; Nowicki, A.; Sawicki, A. Detection of bone disease with ultrasound—Comparison with bone densitometry. *Ultrasonics* **2000**, *38*, 693–697. [CrossRef] [PubMed]

287. Hoffmeister, B.K.; Jones, C.I., 3rd; Caldwell, G.J.; Kaste, S.C. Ultrasonic characterization of cancellous bone using apparent integrated backscatter. *Phys. Med. Biol.* **2006**, *51*, 2715–2727. [CrossRef] [PubMed]

288. Hoffmeister, B.K.; Johnson, D.P.; Janeski, J.A.; Keedy, D.A.; Steinert, B.W.; Viano, A.M.; Kaste, S.C. Ultrasonic characterization of human cancellous bone in vitro using three different apparent backscatter parameters in the frequency range 0.6–15 MHz. *IEEE Trans. Ultrason. Ferroelectr. Freq. Control* **2008**, *55*, 1442–1452. [CrossRef] [PubMed]

289. Karjalainen, J.P.; Töyräs, J.; Riekkinen, O.; Hakulinen, M.; Jurvelin, J. Ultrasound backscatter imaging provides frequency-dependent information on structure, composition and mechanical properties of human trabecular bone. *Ultrasound Med. Biol.* **2009**, *35*, 1376–1384. [CrossRef] [PubMed]

290. Jiang, Y.; Liu, C.; Li, R.; Wang, W.; Ding, H.; Qi, Q.; Ta, D.; Dong, J.; Wang, W. Analysis of apparent integrated backscatter coefficient and backscattered spectral centroid shift in calcaneus *in vivo* for the ultrasonic evaluation of osteoporosis. *Ultrasound Med. Biol.* **2014**, *40*, 1307–1317. [CrossRef] [PubMed]

291. Li, Y.; Li, B.; Xu, F.; Liu, C.; Ta, D.; Wang, W. Ultrasonic backscatter measurements at the calcaneus: An *in vivo* study. *Measurement* **2018**, *122*, 128–134. [CrossRef]

292. Di Paola, M.; Gatti, D.; Viapiana, O.; Cianferotti, L.; Cavalli, L.; Caffarelli, C.; Conversano, F.; Quarta, E.; Pisani, P.; Girasole, G.; et al. Radiofrequency echo-graphic multispectrometry compared with dual X-ray absorptiometry for osteoporosis diagnosis on lumbar spine and femoral neck. *Osteoporos. Int.* **2019**, *30*, 391–402. [CrossRef] [PubMed]

293. Cortet, B.; Dennison, E.; Diez-Perez, A.; Locquet, M.; Muratore, M.; Nogués, X.; Ovejero Crespo, D.; Quarta, E.; Brandi, M.L. Radiofrequency Echographic Multi Spectrometry (REMS) for the diagnosis of osteoporosis in a European multicenter clinical context. *Bone* **2021**, *143*, 115786. [CrossRef] [PubMed]

294. Amorim, D.M.R.; Sakane, E.N.; Maeda, S.S.; Castro, M.L. New technology REMS for bone evaluation compared to DXA in adult women for the osteoporosis diagnosis: A real-life experience. *Arch. Osteoporos.* **2021**, *16*, 175. [CrossRef]

295. Nowakowska-Płaza, A.; Wroński, J.; Płaza, M.; Sudoł-Szopińska, I.; Głuszko, P. Diagnostic agreement between radiofrequency echographic multispectrometry and dual-energy X-ray absorptiometry in the assessment of osteoporosis in a Polish group of patients. *Pol. Arch. Intern. Med.* **2021**, *131*, 840–847. [CrossRef] [PubMed]

296. Pisani, P.; Greco, A.; Conversano, F.; Renna, M.D.; Casciaro, E.; Quarta, L.; Costanza, D.; Muratore, M.; Casciaro, S. A quantitative ultrasound approach to estimate bone fragility: A first comparison with dual X-ray absorptiometry. *Meas. Phys. Educ. Exerc. Sci.* **2017**, *101*, 243–249. [CrossRef]

297. Roux, C.; Roberjot, V.; Porcher, R.; Kolta, S.; Dougados, M.; Laugier, P. Ultrasonic backscatter and transmission parameters at the os calcis in postmenopausal osteoporosis. *J. Bone Min. Res.* **2001**, *16*, 1353–1362. [CrossRef] [PubMed]

298. Pisani, P.; Conversano, F.; Muratore, M.; Adami, G.; Brandi, M.; Caffarelli, C.; Casciaro, E.; Di Paola, M.; Franchini, R.; Gatti, D.; et al. Fragility Score: A REMS-based indicator for the prediction of incident fragility fractures at 5 years. *Aging Clin. Exp. Res.* **2023**, *35*, 763–773. [CrossRef] [PubMed]

299. Adami, G.; Arioli, G.; Bianchi, G.; Brandi, M.L.; Caffarelli, C.; Cianferotti, L.; Gatti, D.; Girasole, G.; Gonnelli, S.; Manfredini, M.; et al. Radiofrequency echographic multi spectrometry for the prediction of incident fragility fractures: A 5-year follow-up study. *Bone* **2020**, *134*, 115297. [CrossRef] [PubMed]

300. Hoffmeister, B.K.; Lawler, B.C.; Viano, A.M.; Mobley, J. Effect of transducer po-sition on ultrasonic backscatter measurements of cancellous bone. *J. Acoust. Soc. Am.* **2023**, *154*, 2858–2868. [CrossRef] [PubMed]

301. Bi, D.; Dai, Z.; Liu, D.; Wu, F.; Liu, C.; Li, Y.; Li, B.; Li, Z.; Li, Y.; Ta, D. Ultrasonic backscatter measurements of human cortical and trabecular bone densities in a head-down bed-rest study. *Ultrasound Med. Biol.* **2021**, *47*, 2404–2415. [CrossRef] [PubMed]

302. Laugier, P.; Novikov, V.; Elmann-Larsen, B.; Berger, G. Quantitative ultrasound imaging of the calcaneus: Precision and variations during a 120-day bed rest. *Calcif. Tissue Int.* **2000**, *66*, 16–21. [CrossRef] [PubMed]

303. Liu, C.; Li, B.; Li, Y.; Mao, W.; Chen, C.; Zhang, R.; Ta, D. Ultrasonic backscatter difference measurement of bone health in preterm and term newborns. *Ultrasound Med. Biol.* **2020**, *46*, 305–314. [CrossRef] [PubMed]

304. Mao, W.; Du, Y.; Liu, C.; Li, B.; Ta, D.; Chen, C.; Zhang, R. Ultrasonic backscatter technique for assessing and monitoring neonatal cancellous bone status *in vivo*. *IEEE Access* **2019**, *7*, 157417–157426. [CrossRef]

305. Liu, C.-R.; Niu, H.-J.; Pu, F.; Wang, L.; Sun, L.-W.; Fan, Y.-B.; Li, D.-Y. The effect of physical loading on calcaneus quantitative ultrasound measurement: A cross-section study. *BMC Musculoskelet. Disord.* **2012**, *13*, 70. [CrossRef] [PubMed]

306. Bowman, S.M.; Zeind, J.; Gibson, L.J.; Hayes, W.C.; McMahon, T.A. The tensile behavior of demineralized bovine cortical bone. *J. Biomech.* **1996**, *29*, 1497–1501. [CrossRef] [PubMed]

307. Wright, T.M.; Vosburgh, F.; Burstein, A.H. Permanent deformation of compact bone monitored by acoustic emission. *J. Biomech.* **1981**, *14*, 405–409. [CrossRef] [PubMed]

308. Jones, B.; Langton, C.M.; Robertson, A.; Tippett, V.; Wearing, S.C. Calcaneal ultrasound attenuation as a predictor of bone density: Does the region of interest or loading influence the repeatability of measurement? *J. Sci. Med. Sport.* **2021**, *24*, 68–69. [CrossRef]

309. Chappard, C.; Berger, G.; Roux, C.; Laugier, P. Ultrasound measurement on the calcaneus influence of immersion time and rotation of the foot. *Osteoporos. Int.* **1999**, *9*, 318–326. [CrossRef] [PubMed]

310. Johansen, A.; Stone, M.D. The effect of ankle oedema on bone ultrasound assessment at the heel. *Osteoporos. Int.* **1997**, *7*, 44–47. [CrossRef] [PubMed]

311. Kotzki, P.O.; Buyck, D.; Hans, D.; Thomas, E.; Bonnel, F.; Favier, F.; Meunier, P.J.; Rossi, M. Influence of fat on ultrasound measurements of the os calcis. *Calcif. Tissue Int.* **1994**, *54*, 91–95. [CrossRef] [PubMed]

312. Evans, W.D.; Jones, E.A.; Owen, G.M. Factors affecting the *in vivo* precision of broad-band ultrasonic attenuation. *Phys. Med. Biol.* **1995**, *40*, 137–151. [CrossRef] [PubMed]

313. Chappard, C.; Camus, E.; Lefebvre, F.; Guillot, G.; Bittoun, J.; Berger, G.; Laugier, P. Evaluation of error bounds on calcaneal speed of sound caused by surrounding soft tissue. *J. Clin. Densitom.* **2000**, *3*, 121–131. [CrossRef] [PubMed]

314. Njeh, C.F.; Boivin, C.M.; Langton, C.M. The role of ultrasound in the assessment of osteoporosis: A review. *Osteoporos. Int.* **1997**, *7*, 7–22. [CrossRef] [PubMed]

315. Hoffmeister, B.K.; Verdonk, E.D.; Wickline, S.A.; Miller, J.G. Effect of collagen on the anisotropy of quasi-longitudinal mode ultrasonic velocity in fibrous soft tissues: A compari-son of fixed tendon and fixed myocardium. *J. Acoust. Soc. Am.* **1994**, *96*, 1957–1964. [CrossRef] [PubMed]

316. Wearing, S.C.; Hooper, S.L.; Smeathers, J.E.; Pourcelot, P.; Crevier-Denoix, N.; Brauner, T. Tendinopathy alters ultrasound transmission in the patellar tendon during squatting. *Scand. J. Med. Sci. Sports* **2016**, *26*, 1415–1422. [CrossRef] [PubMed]

317. Wulf, M.; Wearing, S.C.; Hooper, S.L.; Smeathers, J.E.; Horstmann, T.; Brauner, T. Achilles tendon loading patterns during barefoot walking and slow running on a treadmill: An ultrasonic propagation study. *Scand. J. Med. Sci. Sports* **2015**, *25*, 868–875. [CrossRef] [PubMed]

318. Wearing, S.C.; Hooper, S.L.; Locke, S.; Smeathers, J.E. Non-invasive clinical measurement of the viscoelastic properties of tendon using acoustic wave transmission. *Dtsch. Z. Sport.* **2013**, *64*, 148.

319. Wulf, M.; Shanker, M.; Schuetz, M.; Lutz, M.; Langton, C.M.; Hooper, S.L.; Smeathers, J.E.; Brauner, T.; Wearing, S.C. Lower material stiffness in rupture-repaired Achilles tendon during walking: Transmission-mode ultrasound for post-surgical tendon evaluation. *Knee Surg. Sports Traumatol. Arthrosc.* **2018**, *26*, 2030–2037. [CrossRef] [PubMed]

320. Wearing, S.C.; Reed, L.; Hooper, S.L.; Bartold, S.; Smeathers, J.E.; Brauner, T. Running shoes increase Achilles tendon load in walking: An acoustic propagation study. *Med. Sci. Sports Exerc.* **2014**, *46*, 1604–1609. [CrossRef] [PubMed]

321. Wulf, M.; Wearing, S.C.; Hooper, S.L.; Bartold, S.; Reed, L.; Brauner, T. The effect of an in-shoe orthotic heel lift on loading of the Achilles tendon during shod walking. *J. Orthop. Sports Phys. Ther.* **2016**, *46*, 79–86. [CrossRef] [PubMed]

322. Brauner, T.; Hooper, S.; Horstmann, T.; Wearing, S. Effects of footwear and heel elevation on tensile load in the Achilles tendon during treadmill walking. *Footwear Sci.* **2018**, *10*, 39–46. [CrossRef]

323. Reed, L.; Brauner, T.; Horstmann, T.; Wearing, S.C. Is the energy loss of footwear related to Achilles tendon loading during treadmill walking? *Footwear Sci.* **2023**, *15*, 103–104. [CrossRef]

324. Neptune, R.R.; Sasaki, K.; Kautz, S.A. The effect of walking speed on muscle function and mechanical energetics. *Gait Posture* **2008**, *28*, 135–143. [CrossRef] [PubMed]

325. Wearing, S.C.; Davis, I.S.; Brauner, T.; Hooper, S.L.; Horstmann, T. Do habitual foot-strike patterns in running influence functional Achilles tendon properties during gait? *J. Sport. Sci.* **2019**, *37*, 2735–2743. [CrossRef] [PubMed]

326. Vergari, C.; Pourcelot, P.; Ravary-Plumioen, B.; Dupays, A.G.; Denoix, J.M.; Mitton, D.; Laugier, P.; Crevier-Denoix, N. First application of axial speed of sound to follow up injured equine tendons. *Ultrasound Med. Biol.* **2012**, *38*, 162–167. [CrossRef] [PubMed]

327. Baxter, J.R.; Corrigan, P.; Hullfish, T.J.; O'Rourke, P.; Silbernagel, K.G. Exercise progression to incrementally load the Achilles tendon. *Med. Sci. Sports Exerc.* **2021**, *53*, 124–130. [CrossRef] [PubMed]

328. Farley, C.T.; Blickhan, R.; Saito, J.; Taylor, C.R. Hopping frequency in humans: A test of how springs set stride frequency in bouncing gaits. *J. Appl. Physiol.* **1991**, *71*, 2127–2132. [CrossRef] [PubMed]

329. Farley, C.T.; Morgenroth, D.C. Leg stiffness primarily depends on ankle stiffness during human hopping. *J. Biomech.* **1999**, *32*, 267–273. [CrossRef] [PubMed]

330. Hobara, H.; Inoue, K.; Omuro, K.; Muraoka, T.; Kanosue, K. Determinant of leg stiffness during hopping is frequency-dependent. *Eur. J. Appl. Physiol.* **2011**, *111*, 2195–2201. [CrossRef] [PubMed]

331. Abe, H.; Hayashi, K.; Sato, H. *Data Book on Mechanical Properties of Living Cells, Tissues, and Organs*; Springer: New York, NY, USA, 1996.

332. Frohm, A.; Halvorsen, K.; Thorstensson, A. Patellar tendon load in different types of eccentric squats. *Clin. Biomech.* **2007**, *22*, 704–711. [CrossRef] [PubMed]

333. Ellis, M.I.; Seedhom, B.B.; Wright, V.; Dowson, D. An evaluation of the ratio between the tensions along the quadriceps tendon and the patellar ligament. *Eng. Med.* **1980**, *9*, 189–194. [CrossRef]

334. Uhthoff, H.K.; Sarkar, K. Classification and definition of tendinopathies. *Clin. Sports Med.* **1991**, *10*, 707–720. [CrossRef] [PubMed]

335. Jozsa, L.; Reffy, A.; Kannus, P.; Demel, S.; Elek, E. Pathological alterations in human tendons. *Arch. Orthop. Trauma. Surg.* **1990**, *110*, 15–21. [CrossRef] [PubMed]

336. Kannus, P.; Józsa, L. Histopathological changes preceding spontaneous rupture of a tendon. A controlled study of 891 patients. *J. Bone Jt. Surg.* **1991**, *73A*, 1507–1525. [CrossRef]

337. Snedeker, J.G.; Foolen, J. Tendon injury and repair—A perspective on the basic mechanisms of tendon disease and future clinical therapy. *Acta Biomater.* **2017**, *63*, 18–36. [CrossRef] [PubMed]

338. Steinmann, S.; Pfeifer, C.G.; Brochhausen, C.; Docheva, D. Spectrum of tendon pathologies: Triggers, trails and end-state. *Int. J. Mol. Sci.* **2020**, *21*, 844. [CrossRef] [PubMed]

339. Vergari, C.; Pourcelot, P.; Ravary-Plumioën, B.; Dupays, A.G.; Jacquet, S.; Audigié, F.; Denoix, J.M.; Laugier, P.; Mitton, D.; Crevier-Denoix, N. Axial speed of sound for the monitoring of injured equine tendons: A preliminary study. *J. Biomech.* **2012**, *45*, 53–58. [CrossRef] [PubMed]

340. Wiesinger, H.P.; Seynnes, O.R.; Kösters, A.; Müller, E.; Rieder, F. Mechanical and material tendon properties in patients with proximal patellar tendinopathy. *Front. Physiol.* **2020**, *11*, 704. [CrossRef] [PubMed]

341. Reid, D.; McNair, P.J.; Johnson, S.; Potts, G.; Witvrouw, E.; Mahieu, N. Electromyographic analysis of an eccentric calf muscle exercise in persons with and without Achilles tendinopathy. *Phys. Ther. Sport.* **2012**, *13*, 150–155. [CrossRef]

342. Rosso, C.; Vavken, P.; Polzer, C.; Buckland, D.M.; Studler, U.; Weisskopf, L.; Lottenbach, M.; Müller, A.M.; Valderrabano, V. Long-term outcomes of muscle volume and Achilles tendon length after Achilles tendon ruptures. *Knee Surg. Sports Traumatol. Arthrosc.* **2013**, *21*, 1369–1377. [CrossRef] [PubMed]

343. Horstmann, T.; Lukas, C.; Merk, J.; Brauner, T.; Mündermann, A. Defcits 10-years after Achilles tendon repair. *Int. J. Sports Med.* **2012**, *33*, 474–479. [CrossRef] [PubMed]

344. Chang, Y.J.; Kulig, K. The neuromechanical adaptations to Achilles tendinosis. *J. Physiol.* **2015**, *593*, 3373–3387. [CrossRef] [PubMed]

345. Nilsson-Helander, K.; Thomeé, R.; Grävare-Silbernagel, K.; Thomeé, P.; Faxén, E.; Eriksson, B.I.; Karlsson, J. The Achilles tendon total rupture score (ATRS) development and validation. *Am. J. Sports Med.* **2007**, *35*, 421–426. [CrossRef]

346. Cook, J.L.; Purdam, C.R. The challenge of managing tendinopathy in competing athletes. *Br. J. Sports Med.* **2014**, *48*, 506–509. [CrossRef] [PubMed]

347. Reinschmidt, C.; Nigg, B.M. Influence of heel height on ankle joint moments in running. *Med. Sci. Sports Exerc.* **1995**, *27*, 410–416. [CrossRef] [PubMed]

348. Dixon, S.J.; Kerwin, D.G. The influence of heel lift manipulation on achilles tendon loading in running. *J. Appl. Biomech.* **1998**, *14*, 374–389. [CrossRef]

349. Farris, D.J.; Buckeridge, E.; Trewartha, G.; McGuigan, M.P. The effects of orthotic heel lifts on Achilles tendon force and strain during running. *J. Appl. Biomech.* **2012**, *28*, 511–519. [CrossRef] [PubMed]

350. Dixon, S.J.; Kerwin, D.G. Variations in Achilles tendon loading with heel lift intervention in heel-toe runners. *J. Appl. Biomech.* **2002**, *18*, 321–331. [CrossRef]

351. Braunstein, B.; Arampatzis, A.; Eysel, P.; Brüggemann, G.-P. Footwear affects the gearing at the ankle and knee joints during running. *J. Biomech.* **2010**, *43*, 2120–2125. [CrossRef] [PubMed]

352. Tamura, Y.; Hatta, I.; Matsuda, T.; Sugi, H.; Tsuchiya, T. Changes in muscle stiffness during contraction recorded using ultrasonic waves. *Nature* **1982**, *299*, 631–633. [CrossRef]

353. Hatta, I.; Sugi, H.; Tamura, Y. Stiffness changes in frog skeletal muscle during contraction recorded using ultrasonic waves. *J. Physiol.* **1988**, *403*, 193–209. [CrossRef] [PubMed]

354. Huxley, A.F. Muscle structure and theories of contraction. *Prog. Biophys. Biophys. Chem.* **1957**, *7*, 255–318. [CrossRef]

355. Topchyan, A.; Tatarinov, A.; Sarvazyan, N.; Sarvazyan, A. Ultrasound velocity in human muscle *in vivo*: Perspective for edema studies. *Ultrasonics* **2006**, *44*, 259–264. [CrossRef]

356. Utter, A.C.; McAnulty, S.R.; Sarvazyan, A.; Query, M.C.; Landram, M.J. Evaluation of ultrasound velocity to assess the hydration status of wrestlers. *J. Strength. Cond. Res.* **2010**, *24*, 1451–1457. [CrossRef] [PubMed]

357. Ruby, L.; Sanabria, S.J.; Saltybaeva, N.; Frauenfelder, T.; Alkadhi, H.; Rominger, M.B. Comparison of ultrasound speed-of-sound of the lower extremity and lumbar muscle assessed with computed tomography for muscle loss assessment. *Medicine* **2021**, *100*, e25947. [CrossRef] [PubMed]

358. Rau, R.; Unal, O.; Schweizer, D.; Vishnevskiy, V.; Goksel, O. Frequency-dependent attenuation reconstruction with an acoustic reflector. *Med. Image Anal.* **2021**, *67*, 101875. [CrossRef] [PubMed]

359. Korta Martiartu, N.; Simute, S.; Jaeger, M.; Frauenfelder, T.; Rominger, M.B. Toward speed-of-sound anisotropy quantification in muscle with pulse-echo ultrasound. *IEEE Trans. Ultrason. Ferroelectr. Freq. Control* **2022**, *69*, 2499–2511. [CrossRef] [PubMed]

360. Ruby, L.; Sanabria, S.; Martini, K.; Frauenfelder, T.; Jukema, G.N.; Goksel, O.; Rominger, M.B. Quantification of immobilization-induced changes in human calf muscle using speed-of-sound ultrasound: An observational pilot study. *Medicine* **2021**, *100*, e23576. [CrossRef] [PubMed]

361. Ruby, L.; Kunut, A.; Nakhostin, D.N.; Finkenstaedt, T.; Frauenfelder, T.; Sanabria, S.J.; Rominger, M.B. Speed of sound ultrasound: Comparison with proton density fat fraction assessed with Dixon MRI for fat content quantification of the lower extremity. *Eur. Radiol.* **2020**, *30*, 5272–5280. [CrossRef] [PubMed]

362. Marsh, R.L. Speed of sound in muscle for use in sonomicrometry. *J. Biomech.* **2016**, *49*, 4138–4141. [CrossRef] [PubMed]

363. Pham, T.-L.; Minonzio, J.-G.; Talmant, M.; Laugier, P. Impact of a multi-frequency sequence of measurements on first arriving signal velocity on a bone plate model. In Proceedings of the IEEE International Ultrasonics Symposium, Rome, Italy, 20–23 September 2009; pp. 574–577.

364. Muller, M.; Mitton, D.; Moilanen, P.; Bousson, V.; Talmant, M.; Laugier, P. Prediction of bone mechanical properties using QUS and pQCT: Study of the human distal radius. *Med. Eng. Phys.* **2008**, *30*, 761–767. [CrossRef] [PubMed]

365. Martiartu, N.K.; Boehm, C.; Fichtner, A. 3-D wave-equation-based finite-frequency tomog-raphy for ultrasound computed tomography. *IEEE Trans. Ultrason. Ferroelectr. Freq. Control* **2020**, *67*, 1332–1343. [CrossRef] [PubMed]

366. Wu, X.; Li, Y.; Su, C.; Li, P.; Wang, X.; Lin, W. Ultrasound computed tomography based on full waveform inversion with source directivity calibration. *Ultrasonics* **2023**, *132*, 107004. [CrossRef] [PubMed]

367. Fincke, J.; Zhang, X.; Shin, B.; Ely, G.; Anthony, B.W. Quantitative sound speed imaging of cortical bone and soft tissue: Results from observational data sets. *IEEE Trans. Med. Imaging* **2022**, *41*, 502–514. [CrossRef] [PubMed]

368. Afrakhteh, S.; Behnam, H. Efficient synthetic transmit aperture ultrasound based on tensor completion. *Ultrasonics* **2021**, *117*, 106553. [CrossRef] [PubMed]

369. Ren, D.; Yin, Y.; Li, C.; Chen, R.; Shi, J. Recent advances in flexible ultrasonic transducers: From materials optimization to imaging applications. *Micromachines* **2023**, *14*, 126. [CrossRef] [PubMed]

370. Du, W.; Zhang, L.; Suh, E.; Lin, D.; Marcus, C.; Ozkan, L.; Ahuja, A.; Fernandez, S.; Shuvo, I.I.; Sadat, D.; et al. Conformable ultrasound breast patch for deep tissue scanning and imaging. *Sci. Adv.* **2023**, *9*, 5325. [CrossRef] [PubMed]

371. Xue, X.; Zhang, B.; Moon, S.; Xu, G.X.; Huang, C.C.; Sharma, N.; Jiang, X. Development of a wearable ultrasound transducer for sensing muscle activities in assistive robotics applications. *Biosensors* **2023**, *13*, 134. [CrossRef]

372. Hu, H.; Ma, Y.; Gao, X.; Song, D.; Li, M.; Huang, H.; Qian, X.; Wu, R.; Shi, K.; Ding, H.; et al. Stretchable ultrasonic arrays for the 3-dimensional mapping of the modulus of deep tissue. *Nat. Biomed. Eng.* **2023**, *7*, 1321–1334. [CrossRef] [PubMed]